

Formation and Regulation of Calcium Sparks on a Nonlinear Spatial Network of Ryanodine Receptors

Tian-Tian Li,^{1, a)} Zhong-Xue Gao,^{1, a)} Zuo-Ming Ding,¹ Han-Yu Jiang,^{1, b)} and Jun He^{1, b)}

School of Physics and Technology, Nanjing Normal University, Nanjing 210097, China

(*Electronic mail: jianghy@njnu.edu.cn)

(*Electronic mail: junhe@njnu.edu.cn)

(Dated: 14 July 2025)

Accurate regulation of calcium release is essential for cellular signaling, with the spatial distribution of ryanodine receptors (RyRs) playing a critical role. In this study, we present a nonlinear spatial network model that simulates RyR spatial organization to investigate calcium release dynamics by integrating RyR behavior, calcium buffering, and calsequestrin (CSQ) regulation. The model successfully reproduces calcium sparks, shedding light on their initiation, duration, and termination mechanisms under clamped calcium conditions. Our simulations demonstrate that RyR clusters act as on-off switches for calcium release, producing short-lived calcium quarks and longer-lasting calcium sparks based on distinct activation patterns. Spark termination is governed by calcium gradients and stochastic RyR dynamics, with CSQ facilitating RyR closure and spark termination. We also uncover the dual role of CSQ as both a calcium buffer and a regulator of RyRs. Elevated CSQ levels prolong calcium release due to buffering effects, while CSQ-RyR interactions induce excessive refractoriness, a phenomenon linked to pathological conditions such as ventricular arrhythmias. Dysregulated CSQ function disrupts the on-off switching behavior of RyRs, impairing calcium release dynamics. These findings provide new insights into RyR-mediated calcium signaling, highlighting CSQ's pivotal role in maintaining calcium homeostasis and its implications for pathological conditions. This work advances the understanding of calcium spark regulation and underscores its significance for cardiomyocyte function.

Calcium release events, particularly calcium sparks mediated by ryanodine receptors, are vital for cellular signaling, underpinning processes like muscle contraction and neuronal communication. Advances in super-resolution imaging have revealed the intricate spatial organization of RyRs, highlighting their crucial role in calcium dynamics. This study introduces a nonlinear spatial network model to simulate calcium release, incorporating the effects of RyR cluster distribution and the regulatory role of calsequestrin. By replicating spontaneous and evoked calcium sparks, the model elucidates how RyR transition rates, calcium concentrations, and CSQ buffering influence spark duration and refractoriness. These insights shed light on calcium signaling regulation and its implications for diseases like ventricular tachycardia.

initiating calcium release within entire RyR clusters, acting as an on-off switch.^{8,9} When this occurs, spontaneous calcium sparks are governed by calcium-induced calcium release (CICR) mechanisms.¹⁰ Similarly, calcium release of L-type calcium channels (LCCs) can also evoke calcium sparks, exhibiting experimental behavior comparable to spontaneous sparks.^{11,12} These localized calcium sparks play a pivotal role in various physiological processes, including excitation-contraction coupling in cardiac and muscle cells, as well as synaptic transmission in neurons.^{7,13–15} Moreover, calcium sparks form the fundamental building blocks of larger-scale calcium waves. Thus, calcium sparks occupy a central position within the hierarchical framework governing calcium dynamics within cells, necessitating a profound understanding of their formation and regulation to elucidate the mechanisms of calcium release and their implications in disease pathogenesis.

I. INTRODUCTION

Calcium release events (CREs), particularly calcium sparks, mediated by RyRs on the junctional sarcoplasmic reticulum (JSR), are crucial for sustaining cellular functions through complex calcium signaling pathways, especially in cardiac and skeletal muscle cells.^{1–7} Under physiological conditions, RyRs exhibit a low probability of opening, whereas pathological states can lead to malfunction-induced activation. This activation of RyRs has a minimal likelihood of

Early investigations into calcium release often lacked explicit representations of cluster structures and relied on mean-field assumptions, which overlooked CICR interactions among RyRs within a cluster.^{16,17} This mean-field approach failed to capture the localized dynamics of calcium release, as evidenced by numerous studies that highlighted its limitations.^{16–23} More recent research has addressed these concerns by incorporating explicit CICR mechanisms within the cluster structure.^{22–26} Similarly, the spatial distribution of inositol 1,4,5-trisphosphate receptors (IP3R), another type of calcium channel, has also been shown to be crucial for understanding their functional properties.^{6,27–30} Advanced imaging techniques, such as electron tomography and single-molecule localization microscopy, have revealed that RyR clusters exhibit irregular shapes, varying sizes, and a stochastic distribution of RyRs, contrary to earlier assumptions of densely

^{a)}These authors have contributed equally to this work.

^{b)}Corresponding author

packed, lattice-like configurations.^{31–35} This intricate organization further underscores the importance of incorporating cluster-specific mechanisms into calcium release models.

Pioneering efforts in the literature have studied calcium signal transduction on networks of calcium channels, incorporating the spatial distribution characteristics of RyRs. Notably, Walker et al.^{24,25} introduced an adjacency matrix for modeling calcium release in the heart, simulating lattice-like configurations of RyRs within clusters. Further approaches, as explored in the literature^{21,22,36} and in our previous studies,^{37,38} conceptualized RyRs as nodes of a network interconnected by the diffusion of calcium ions. Given these advancements, it is intriguing to study calcium release with new experimental information on RyR spatial distribution, which has not been previously considered in investigations of calcium signaling.

Calcium sparks occur in the dyad between the JSR and the transverse tubule. These sparks are influenced not only by the spatial distribution of RyRs but also by calcium concentrations and buffers, particularly CSQ, which plays a critical role in calcium release.³⁹ Calcium sparks in transgenic mice with overexpressed or underexpressed CSQ exhibit longer or shorter duration of calcium sparks, respectively, highlighting the crucial role of CSQ in modulating RyR activity.⁴⁰ The authors suggested that the predominant effects of CSQ on JSR calcium release are due to its buffering actions inside the JSR. CSQ regulates calcium sparks not only by acting as a buffer but also by influencing RyR activity.^{41–43} Lipid bilayer experiments have shown that RyR channel activity is modulated by the interaction of CSQ with the auxiliary proteins triadin and junctin.^{44–46} Specifically, CSQ dissociates from RyR under high JSR calcium concentration, enhancing RyR sensitivity to Ca^{2+} in the dyadic cleft. Conversely, low JSR calcium concentration causes CSQ binding to RyR, diminishing sensitivity. Raising the luminal calcium concentration from 20 μM to 5 mM, which binds to and polymerizes CSQ, leads to an enhanced open probability of the channels.⁴⁷

These findings highlight the intricate regulatory roles of CSQ in calcium signaling dynamics, with increasing attention being paid to their relevance to diseases such as catecholaminergic polymorphic ventricular tachycardia (CPVT) in recent years.^{43,48,49} However, there is still a need for more simulation and theoretical analysis to fully understand this phenomenon. Restrepo et al. simulated the effect of CSQ by using CSQ-bound and CSQ-unbound states,⁵⁰ revealing its contribution to the excessive refractoriness of calcium sparks.⁵¹ However, their simulation, which considered more calcium cycling mechanisms, and a realistic number of dyads, each with a realistic number of RyR channels, makes it computationally difficult to incorporate the spatial distribution of RyRs or the explicit CICR mechanism.⁵⁰

Incorporating spatial distributions into the RyR transition model offers a novel pathway for calcium signaling research, particularly through the application of recent experimental data,^{32–35} which remain underexplored in CRE studies. Our goal is to simulate CREs to assess whether calcium sparks with experimentally observed properties, specifically their on-off switching behavior, can be accurately reproduced. By utilizing this model, we aim to explore the regulation of cal-

cium sparks through clamped calcium concentrations in the myoplasm and network sarcoplasmic reticulum (NSR). Additionally, we plan to investigate the explicit influence of calsequestrin on RyR clusters,^{40–43,51} especially by incorporating spatial RyR distributions that are underrepresented in existing literature. This approach is expected to provide deeper insights into the buffering mechanisms of calsequestrin and its impact on RyR function, thereby offering multiple directions for follow-up studies in cellular signaling regulation.

In this study, we introduce a spatial network model in Section II to incorporate the spatial distribution of RyRs. We account for CSQ binding and unbinding states to capture its effects on RyR activity. Additionally, RyR transition rates are determined by fitting experimental data. The calcium exchange and calcium buffers are also considered to establish a mechanism for simulating calcium release through RyRs on JSR. In Section III, the simulation of CREs aims to replicate its on-off switch characteristic, specifically focusing on the formation of calcium sparks with spontaneous and evoked activations. In Section IV, we discuss the regulation of calcium sparks by opening rate and clamped calcium concentrations in the myoplasm and NSR concerning the duration and open RyRs of calcium sparks. Moreover, we investigate the regulation of calcium sparks by CSQ, which affects the opening possibilities of RyRs and acts as a buffer. We use experimental data to elucidate these roles and discuss potential malfunctions in CSQ regulation. The article concludes with discussion and summary in the last section V.

II. MODEL OF CALCIUM RELEASE ON JSR

This study focuses on elucidating the complexities of CREs, particularly calcium sparks, occurring on the JSR. The JSR, a terminal cistern of the sarcoplasmic reticulum containing an array of RyRs, is dispersed randomly around the transverse tubule, forming a subspace (SS) with an average distance of approximately 15 nm as shown in Fig. 1. The release of calcium ions from the JSR into the SS is orchestrated by the controlled opening of RyRs. The state of these receptors, whether open or closed, is contingent upon the local concentrations of calcium ions, denoted as $[\text{Ca}^{2+}]_i^{\text{SS}}$ and $[\text{Ca}^{2+}]_i^{\text{JSR}}$, in the vicinity of each specific i^{th} RyR.

The exchange of calcium ions takes place between the RyR clusters, the myoplasm, and the NSR. In this study, our primary focus is on calcium sparks, which typically last for approximately 20 ms. We do not consider larger-scale CREs such as calcium waves, thus limiting the number of calcium sparks and minimizing the impact on the calcium concentration in the myoplasm $[\text{Ca}^{2+}]^{\text{myo}}$ and the NSR $[\text{Ca}^{2+}]^{\text{NSR}}$. Consequently, we maintain clamped concentrations of $[\text{Ca}^{2+}]^{\text{myo}}$ and $[\text{Ca}^{2+}]^{\text{NSR}}$ at standard values of 0.1 and 1000 μM , respectively.^{2,16} We will also discuss the results obtained with alternative values of $[\text{Ca}^{2+}]^{\text{myo}}$ and $[\text{Ca}^{2+}]^{\text{JSR}}$. This approach aligns with lipid bilayer experiments that utilize clamped calcium concentrations. Compared to the study of Restrepo et al.⁵⁰, which incorporated calcium cycling, our current treatment reduces computational complexity, enabling the inclu-

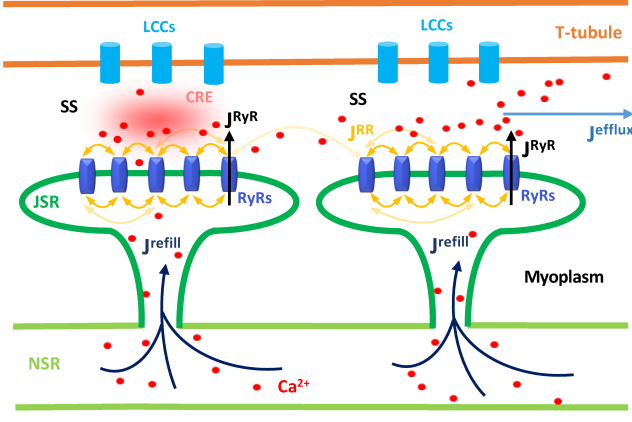


FIG. 1. Schematic representation of the calcium release mechanism. The RyRs, located in the JSR, facilitate the flux of calcium ions (J_i^{RyR}) from the JSR to the SS. Calcium ions also diffuse from other RyRs to a specific RyR i in both the JSR and SS, denoted as a flux J_i^{RR} . These fluxes collectively contribute to CREs occurring within the SS. Calcium ions in the SS can exit into the myoplasm through efflux, represented as J_i^{efflux} . Simultaneously, calcium ions refill the JSR from the NSR, depicted as J_i^{refill} .

sion of the explicit RyR spatial distribution.

The buffering system plays a crucial role in shaping the dynamics of $[\text{Ca}^{2+}]_i^{\text{SS}}$ fluctuations. In this study, we incorporate the impact of calcium buffers and specifically examine the effect of CSQ, a buffer protein found in the JSR, on calcium spark behavior. Taking these factors into consideration, we can formulate the temporal evolution of $[\text{Ca}^{2+}]_i^{\text{SS}}$ and $[\text{Ca}^{2+}]_i^{\text{JSR}}$ as follows,

$$\begin{aligned} \frac{d[\text{Ca}^{2+}]_i^{\text{SS}}}{dt} &= J_i^{\text{RyR}} + J_i^{\text{RR}} - J_i^{\text{efflux}} - J_i^{\text{buffer}}, \\ \frac{d[\text{Ca}^{2+}]_i^{\text{JSR}}}{dt} &= \frac{V^{\text{SS}}}{V^{\text{JSR}}} \beta_i \left(-J_i^{\text{RyR}} + J_i^{\text{RR}} \right) + J_i^{\text{refill}}. \end{aligned} \quad (1)$$

The explicit mechanisms are depicted in Fig. 1, and detailed explanations of each flux will be provided in the subsequent subsections.

A. State Transition of RyRs

RyRs primarily exist in two conformations: open and closed. Numerous studies utilize this two-state model to describe calcium dynamics, where the transition between these states is predominantly driven by calcium concentrations.^{9,21–24} However, RyRs are also regulated by additional factors, such as calmodulin and CSQ. To account for these regulatory complexities, several models have been proposed that expand beyond the two-state paradigm.⁵² In our study, we focus primarily on the role of CSQ in regulating calcium release. Previous work has incorporated the effects of CSQ on RyR transition rates through Ca^{2+} binding at cytosolic activation and inactivation sites.^{53,54} Restrepo et al.⁵⁰ offered a

mechanistic explanation for this phenomenon, later adapted by Sato and Bers into a more comprehensive model with additional refinements.^{55,56} In this model, CSQ binding to RyR complexes notably reduces RyR activity. To represent this regulation, the model distinguishes between two RyR states: those bound to CSQ and those unbound. This approach effectively captures CSQ's modulation of RyR activity and its impact on calcium release dynamics, as detailed in the work by Restrepo et al.⁵⁰

When $[\text{Ca}^{2+}]_i^{\text{JSR}}$ is elevated, it triggers the release of CSQ from the RyR complex, which in turn enhances the sensitivity of RyR to $[\text{Ca}^{2+}]_i^{\text{SS}}$. This phenomenon is shown in Fig. 2, where two distinct states are illustrated: the CSQ-unbound open state (O_u) and the CSQ-unbound closed state (C_u). The opening and closing rates of RyRs, k_O and k_C , are predominantly influenced by the calcium ion concentration in the subspace $[\text{Ca}^{2+}]_i^{\text{SS}}$, located near the RyR.

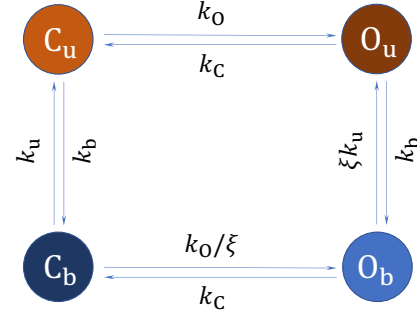


FIG. 2. Schematic representation of transitions of four possible states of a RyR channel: closed CSQ-unbound C_u , open CSQ-unbound O_u , closed CSQ-bound C_b , and open CSQ-bound O_b .

The opening and closing rates of RyRs, k_O and k_C , have been determined empirically through single-channel recordings of rat cardiac RyRs under varying luminal calcium concentration,²³ as replotted in Fig. 3(a) and (b). In the original study,²³ the experimental transition rates were fitted by the following equations:

$$\begin{aligned} k_O^{\text{rat}} &= \min \left[a_O^{\text{rat}} ([\text{Ca}^{2+}]_i^{\text{SS}})^{2.8}, b_O^{\text{rat}} \right], \\ k_C^{\text{rat}} &= \max \left[a_C^{\text{rat}} ([\text{Ca}^{2+}]_i^{\text{SS}})^{-0.5}, b_C^{\text{rat}} \right], \end{aligned} \quad (2)$$

where “min” and “max” indicate the selection of the minimum and maximum of the two values, respectively. The parameters $a_O^{\text{rat}} = 1.262 \times 10^{-3} \text{ s}^{-1} \mu\text{M}^{-2.8}$, $b_O^{\text{rat}} = 700 \text{ s}^{-1}$, $a_C^{\text{rat}} = 7906 \text{ s}^{-1} \mu\text{M}^{0.5}$, and $b_C^{\text{rat}} = 900 \text{ s}^{-1}$ were obtained from the experimental data. Similarly, for sheep, the transition rates were fitted as follows:

$$\begin{aligned} k_O^{\text{sheep}} &= \min \left[a_O^{\text{sheep}} ([\text{Ca}^{2+}]_i^{\text{SS}})^{2.12}, b_O^{\text{sheep}} \right], \\ k_C^{\text{sheep}} &= a_C^{\text{sheep}} ([\text{Ca}^{2+}]_i^{\text{SS}})^{-0.27}, \end{aligned} \quad (3)$$

where the corresponding parameters are $a_O^{\text{sheep}} = 0.1995 \text{ s}^{-1} \mu\text{M}^{-2.12}$, $b_O^{\text{sheep}} = 800 \text{ s}^{-1}$ for opening rate, and $a_C^{\text{sheep}} = 1582 \text{ s}^{-1} \mu\text{M}^{0.27}$ for closing rate. These fitted

opening and closing rates are presented as dotted lines in Fig. 3(a) and (b), respectively.

Typically, the opening rates of RyRs can be expressed using a sigmoid form as:

$$k_O = a_O \frac{([Ca^{2+}]_i^{SS})^n}{([Ca^{2+}]_i^{SS})^n + K^n}, \quad (4)$$

It is similar to the formulations used in other studies.¹⁶ However, these research^{16,17} introduced a cooperative factor into the transition rate to describe the interconnection between RyRs. In this study, we consider the RyRs as nodes in a spatial network, connected through calcium diffusion as a link (see Section II B). Therefore, such a cooperative factor is unnecessary in the current model. After fitting the data, the exponential indices n for rat and sheep are found to be 4 and 2, respectively. The corresponding values of a_O are 816.36 and 1259.1, and K values are 86.96 and 63.35 μM for rat and sheep, respectively. These sigmoid-fitted lines are shown as solid lines in Fig. 3(a), and it can be seen that both forms of fitting, original ones by Cannell et al. and sigmoid, yield comparable results.

The closing rates of RyRs, often treated as constants in previous studies,^{16,17,24} were similarly fitted as constants in our analysis, with values of 1066.8s^{-1} for rats and 810.0s^{-1} for sheep. These values differ from those reported by Cannell et al.²³ primarily due to the different fitting methods employed. This approach not only provides greater flexibility in analyzing the closing rates but also enables the derivation of a sigmoid form for the open probabilities. For clarity, we label these constant closing rates as "sigmoid" in Fig. 3(b).

If we only consider the transitions between two unbound states, the open probability of RyRs P_O for a given calcium concentration can be derived from the opening and closing rates as $k_O/(k_O + k_C)$. Specifically, when using the sigmoid-form opening rate and a constant closing rate, the open probability is given by:

$$P_O = \frac{a_O}{a_O + K^n} \frac{([Ca^{2+}]_i^{SS})^n}{([Ca^{2+}]_i^{SS})^n + \frac{k_C K^n}{a_O + K^n}}, \quad (5)$$

which clearly exhibit as a sigmoid shape, consistent with the behavior observed in prior studies^{17,22,24} and shown in Fig. 3(c).

For rats, the open probability derived from the sigmoid fit remains close to the results obtained by Cannell et al.,²³ except for a slight deviation around 100 μM . However, for sheep, there is a more significant discrepancy, primarily due to the assumption of a constant closing rate in our model. The introduction of a sigmoid-form opening rate allows for more straightforward exploration of how changes in the rates impact RyR behavior. For instance, in Fig. 3, we present a case where the opening rate for rats is halved as $K = 43.48$, which increases the open probability P_O at lower calcium concentrations. Additionally, the impact of a larger closing rate for sheep is explored, revealing a noticeable reduction in P_O . These parameter variations and their effects will be discussed further in the subsequent sections.

In vitro experiments have demonstrated that CSQ forms dimers at calcium concentrations exceeding approximately 500 μM and higher-order polymers at concentrations of a few mM.⁵⁷ Typically, the calcium concentration in the NSR remains high, maintaining $[Ca^{2+}]_i^{JSR}$ at around 1 mM. RyRs are in CSQ-unbound states with heightened sensitivity to Ca^{2+} in the SS. When RyRs are open, calcium ions are released from the JSR into the SS, resulting in a decrease in $[Ca^{2+}]_i^{JSR}$. At low $[Ca^{2+}]_i^{JSR}$ levels, CSQ binds to the triadin/junctin complex, thereby reducing RyR sensitivity.⁴⁴⁻⁴⁶ The open CSQ-bound state (O_b) and closed CSQ-bound state (C_b) are introduced for RyRs with reduced sensitivity. This state introduces lower transition rates, denoted as k_O/ξ , from the closed to the open state, with $\xi = 7.6$.⁵⁰

The binding and unbinding rates of CSQ to the RyRs are dependent on the $[Ca^{2+}]_i^{JSR}$ and the concentration of CSQ, B_{CSQ} , given by,⁵⁰

$$k_b = \hat{M} \tau_b^{-1} B_{CSQ}/B_{CSQ}^0, \quad k_u = \tau_u^{-1}, \quad (6)$$

where the binding and unbinding timescales are $\tau_b = 5$ ms and $\tau_u = 125$ ms, respectively. The relative monomer concentration is,

$$\hat{M} = \frac{(1 + 8\rho B_{CSQ})^{1/2} - 1}{4\rho B_{CSQ}}, \quad \text{with } \rho = \frac{\rho_\infty ([Ca^{2+}]_i^{JSR})^h}{K^h + ([Ca^{2+}]_i^{JSR})^h}. \quad (7)$$

Here, $B_{CSQ}^0 = 400$ μM is the normal concentration, ensuring that k_b approaches τ_b^{-1} for low $[Ca^{2+}]_i^{JSR}$. The parameters in the sigmoid function are chosen as $\rho_\infty = 5 \times 10^3$, $K = 1000$ μM , and $h = 23$.⁵⁰

The actual release of calcium occurs when the RyR is in an open state O_u and O_d , facilitating the flow of calcium ions from the JSR into the subspace. The rate of calcium transfer is determined by the concentration gradient between these two compartments, expressed as:

$$J_i^{\text{RyR}} = \frac{i^{\text{RyR}}}{2FV^{SS}} ([Ca^{2+}]_i^{JSR} - [Ca^{2+}]_i^{SS}) \delta_{i,O_u+O_d}. \quad (8)$$

Here, J_i^{RyR} represents the calcium flux through the RyR and δ_{i,O_u+O_d} means the RyR i stays in one of two open states O_u or O_d . The constant i^{RyR} is chosen to yield a flux of 0.6 pA for an open RyR with a calcium gradient of 1 mM.^{23,58,59} The Faraday constant, denoted as F , is equivalent to 96485 C/mol. The volumes of the subspace and JSR are assigned values of $V^{SS} = 10^{-19}$ L and $V^{JSR} = 2 \times 10^{-18}$ L, respectively.¹⁶

B. Spatial network of RyRs

The CICR mechanism hinges on the diffusion of calcium ions between RyR channels. Upon activation of RyRs, a release of calcium ions transpires, resulting in an increase in calcium concentration and the establishment of a non-uniform distribution of calcium ions within the system. These calcium

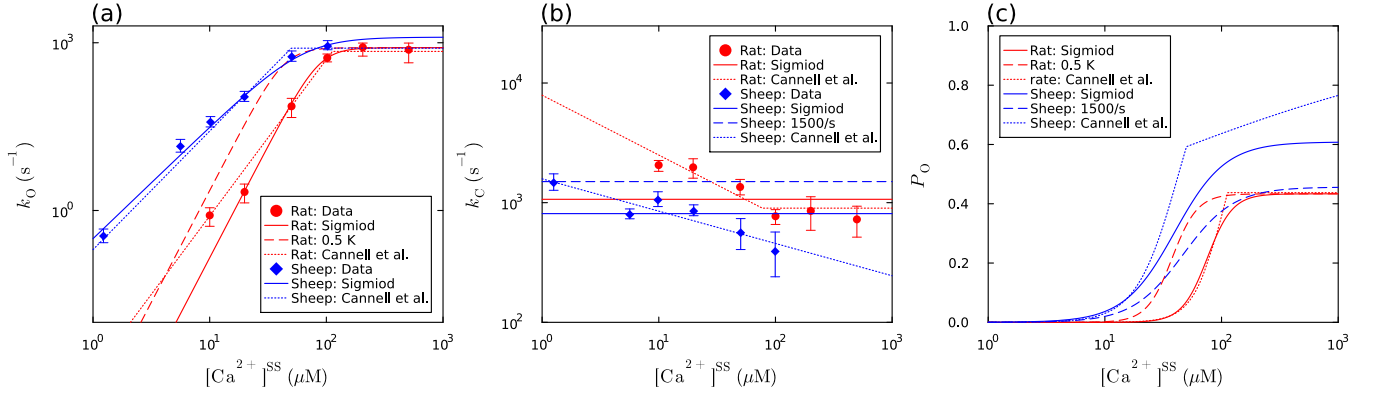


FIG. 3. Transition rates of RyR as a function of calcium concentration $[Ca^{2+}]_i^{SS}$. (a) The opening rate, (b) the closing rate, and (c) the open probabilities. Data points from Cannell et al.²³ are marked as red circles (rat) and blue diamonds (sheep). The dotted lines represent the original fits by Cannell et al.,²³ while the solid lines show the new fits obtained in this study to derive a sigmoid form for RyR open probabilities. The red dashed line shows the result of reducing K to half its value for rats, while the blue dashed line represents the effect of increasing the closing rate to 1500 s^{-1} for sheep.

ions subsequently undergo diffusion driven by concentration gradients as follows,

$$J_i^{RR} = \sum_j A_{ij} ([Ca^{2+}]_j - [Ca^{2+}]_i). \quad (9)$$

Here, J_i^{RR} represents the calcium flux through i^{th} RyR, which is influenced by the difference in calcium concentrations between j^{th} RyR and i^{th} RyR. The strength of connection between two RyRs is captured by an adjacency matrix, denoted as A_{ij} , within the context of a spatial network. This matrix is intrinsically tied to the spatial proximity of the RyRs, effectively mirroring the arrangement of RyR clusters on the JSR. Recent experimental insights, made possible by super-resolution imaging techniques, have uncovered that RyR clusters exhibit irregular, non-compact shapes and are randomly distributed across JSR.^{33–35} Therefore, to faithfully represent the spatial distribution of calcium channels, it is imperative to generate the RyR network based on experimental data.

The existing literature reveals varied experimental findings regarding cluster size (the number of RyRs per cluster) and their frequency distribution, as highlighted in several studies.^{33–35} Generally, smaller clusters are more prevalent than larger ones, following a power-law distribution.^{33–35,60,61} In our previous work,³⁸ we derived a normalized frequency distribution function based on recent experimental data, expressed as:

$$f(x) = 0.991e^{-0.66x} + 0.009e^{-0.017x}, \quad (10)$$

where x denotes the cluster size and $f(x)$ represents the frequency distribution of clusters of that size.

When examining a single cluster, the size can be directly assigned. However, for multiple clusters, the sizes are generated based on the specified frequency distribution. Considering N RyRs, two random numbers, $r_1 \in [0, 1]$ and $r_2 \in [0, n_{\max}]$, are used. To limit the occurrence of overly large clusters in a constrained space, the maximum cluster size is capped at $n_{\max} = 100$, consistent with experimental findings that clusters

exceeding 100 RyRs are rarely observed.^{33–35} If $r_1 < f(r_2)$, r_2 is taken as the cluster size; otherwise, both random numbers are discarded. This procedure repeats until the total number of RyRs equals the total number of channels, N .

In the earlier step, cluster sizes were either randomly determined or explicitly assigned for a single cluster. The next stage involves generating clusters of the specified sizes. According to the literature, the structural arrangement of a cluster is intricate. In this study, we employ the spatial distributions of RyRs proposed by Jayasinghe et al.,³⁴ derived from super-resolution imaging. These findings reveal that clusters are non-compact and possess irregular geometries. Conveniently, the authors of the referenced work also outlined a method for the random generation of clusters, which we directly adopt in this study.

The simulation starts with an initial position $x_1 = (0, 0)$, which is stored as the position of the first RyR in a vector. A random direction θ is then generated, along with a distance r that fluctuates around a mean value of 40 nm, drawn from a Gaussian distribution with a standard deviation of 7.4 nm. This distribution closely aligns with the observed distance characteristics in both mean and variance, as reported by Jayasinghe et al.³⁴ The position updates to $x_2 = x_1 + \Delta x$, where $\Delta x = (r \cos \theta, r \sin \theta)$ represents the displacement. The new position x_2 is added to the vector as the second RyR's position. This process is iterated by generating additional random directions and distances, leading to subsequent position updates, such as x_3 , which are similarly recorded. The procedure continues until the positions of all RyRs in a cluster of the specified size are stored in the vector. As illustrated in Fig. 4(a), this iterative assembly process results in the formation of clusters with irregular gaps, resembling those observed in experiment.³⁴

To randomly distribute the clusters with different sizes in a two-dimensional plane, we follow observations that suggest a random distribution of clusters of various sizes,^{33–35} which is applied here. A square region of side length $l = d \sqrt{N_{\text{cluster}}}$ is considered, where d represents the average distance between

clusters and N_{cluster} denotes the total number of clusters. Previous studies have shown that the nearest neighbor distances have a peak near 200 nm with a long tail.³⁴ In this work, we adopt a mean distance of 250 nm.

For positioning each cluster, two random values in the range $[0, l]$ are generated to define its location, and these are added to the positions of the RyRs in that cluster obtained from the previous step. Since random placement in the plane may cause overlaps, we address this issue by dividing the square region into lattices of $30 \times 30 \text{ nm}^2$. As the positions of the RyRs in a cluster are determined, the corresponding lattices are marked as occupied and cannot be used again. This method ensures that the clusters are randomly distributed without overlap, as shown in Fig. 4(a).

To construct the spatial network, we consider RyRs as nodes. The link between the nodes is abstracted from the calcium diffusion between two RyRs, which depends on the distance between them. In an unbuffered system, the diffusion of Ca^{2+} ions is typically proportional to the reciprocal of the distance to the open RyR, that is $A_{ij} \propto 1/r_{ij}$. However, including calcium buffers near RyRs reduces the concentration of free Ca^{2+} ions and alters their distribution.⁶² Therefore, this relationship serves as an upper bound in formulating Ca^{2+} -mediated RyR-RyR interactions.²² Furthermore, explicit calculations regarding three-dimensional cytoplasmic calcium propagation indicate that calcium diffusion exhibits an exponential dependence on distance, as shown in the work by Hernandez-Hernandez et al.,³⁶ and our previous work.⁶³ The rapid decrease with distance r_{ij} in the exponential decay function aligns with the model of Walker et al., where adjacent RyRs have much stronger connections than those farther away.^{24,25} Hence, we employ an exponential decay function of the spatial distance r_{ij} between two RyRs, incorporating two scaling parameters, τ_{RR} and r_0 , to determine the strength and range of connection between RyRs. The mathematical representation is given by:

$$A_{ij} = \frac{e^{-r_{ij}/r_0}}{\tau_{RR}}. \quad (11)$$

The range scale r_0 is set to 60 nm, roughly equivalent to twice the size of a RyR. This choice is intended to capture the appropriate interaction range between RyRs in the simulation, taking into account their physical dimensions. The parameter τ_{RR} represents the strength of the connection between two RyRs, which in turn reflects the magnitude of the flux or exchange of ions between them. However, this parameter cannot be directly estimated from available experimental data. Given the calcium diffusion constant $D_{\text{Ca}} = 200 \mu\text{m}^2/\text{s}$, we estimate the diffusion time as $\tau_{RR} = r_0^2/2D_{\text{Ca}} \approx 0.01 \text{ ms}$.

Although our primary focus is on a single cluster of RyRs, we now aim to present a spatial network illustrating the randomized distribution of RyRs across multiple clusters. This network provides a clearer representation of clusters with varying sizes. As an illustrative example, Fig. 4 shows a network of 1000 RyRs, successfully replicating the cluster structure observed in previous studies. Different colors are used in the figure to distinguish between the RyR clusters, which exhibit random shapes and sizes. Notably, by adopting the

self-assembly process,³⁴ the clusters show larger gaps, similar to those observed and reported in that reference.

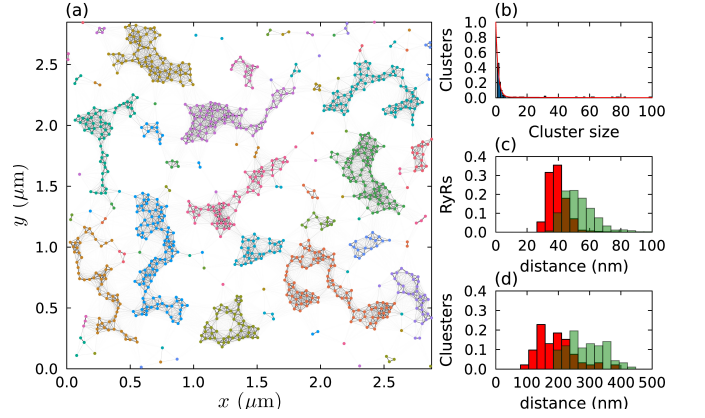


FIG. 4. Randomly generated spatial network. (a) The spatial arrangement with distinct colors denoting different clusters of RyRs. The width and grayscale of the connecting lines between RyRs indicate the strength of their connections as A_{ij} . (b) Comparison of randomly generated cluster size distribution (blue histogram) with the predetermined distribution (red curve) in Eq. (10). (c) Distribution of nearest neighbor distances within clusters: The red bars represent the distribution of nearest neighbor distances within clusters containing five or more RyRs, while the green line represents the average value of the four nearest neighbor distances. (d) Cluster-level analysis: Similar to panel (c) but at the cluster level.

To better understand the spatial distribution of RyRs and evaluate the consistency between our simulations and experimental data, we analyze the distribution of cluster sizes, as shown in Fig. 4(b). This analysis reveals that our model closely adheres to the predetermined cluster size distribution given by Eq. (10), which is based on experimental data.³⁵ Additionally, we examine the spatial relationships between RyRs within clusters by analyzing the nearest neighbor distances. Fig. 4(c) illustrates the distribution of these distances, along with the average of the four nearest neighbor distances. The strong agreement of these metrics with experimental data underscores the accuracy of our model in capturing the spatial arrangement of RyRs. Furthermore, we extend this analysis to explore the distribution of distances between clusters, which follows a long-tail distribution consistent with experimental observations,³⁴ as depicted in Fig. 4(d).

In our model, each RyR is represented as a colored dot in Fig. 4(a) and is abstracted as a node within the spatial network. The connections between RyRs are visually depicted as lines, with the width and grayscale of these lines corresponding to the strength of the connections as A_{ij} in Eq. (11). Notably, the stronger connections within clusters are clearly visible, highlighting their critical role in facilitating calcium release and generating calcium sparks.

C. Exchange of calcium and buffering

In our study, we clamp the calcium concentrations in NSR and myoplasm at constant levels. The resting calcium concentration in the myoplasm, denoted as $[Ca^{2+}]^{myo}$, is approximately $0.1 \mu M$, as determined experimentally.^{2,16} The efflux of calcium ions from the subspace to the myoplasm, represented by J_i^{efflux} , occurs due to the concentration gradient between the SS and myoplasm as,^{16,17,50}

$$J_i^{efflux} = \frac{[Ca^{2+}]_i^{SS} - [Ca^{2+}]^{myo}}{\tau_{efflux}}, \quad (12)$$

where, τ_{efflux} is set as 0.02 ms , which corresponds to diffusion over a distance of approximately 80 nm , the average distance required to exit the proximal space, which has a cylindrical shape with a radius of 200 nm .⁵⁰

As calcium is released from the JSR through the RyRs, the $[Ca^{2+}]_i^{JSR}$ decreases, initiating calcium refilling from the NSR, where the calcium concentration is maintained at 1 mM .^{2,16,17,25} The refill flux (J_i^{refill}) is proportional to the concentration gradient between the NSR and the JSR,^{16,17,50}

$$J_i^{refill} = \frac{[Ca^{2+}]^{NSR} - [Ca^{2+}]_i^{JSR}}{\tau_{refill}}, \quad (13)$$

where the time constant τ_{refill} is chosen as 5 ms .⁵⁰

Within the framework of calcium regulation, calcium ions also interact with calcium buffers, including sarcolemmal (SL) and sarcoplasmic reticulum (SR) membrane buffers, as well as the versatile protein CaM. The characteristics of these buffers can be mathematically described by the equation,^{64,65}

$$J_i^{buffer} = -k_{on}[B][Ca^{2+}]_i + k_{off}([B]_T - [B]_i). \quad (14)$$

In this equation, the rate at which calcium ions bind to the buffer is denoted by k_{on} , while the rate at which they dissociate from the buffer is represented by k_{off} . Moreover, $[B]_T$ and $[B]_i$ signify the total concentration of buffer and the concentration of unbound buffer, respectively. Please refer to Table I for specific values of the constants related to buffering.

TABLE I. Buffering parameters.⁶⁵

Buffer	$[B]_T (\mu M)$	$k_{on} (\mu M^{-1} s^{-1})$	$k_{off} (s^{-1})$
CaM	24	100	38
SR	47	115	100
SL	1124	115	1000

In this research, we concentrate primarily on the modulation of calcium release mediated by CSQ, the principal calcium buffer residing within the JSR. To model this process, we adopt the fast buffering approximation.⁶⁶ While this approximation does not strictly conserve mass, it is acceptable in our context because the calcium concentration is clamped, making mass conservation irrelevant. The β_i factor, appearing in Eq. (1), is defined as per the formulation presented in Restrepo's study,⁵⁰

$$\beta_i(c_i) = \left(1 + \frac{K_C B_{CSQ} n(c_i) + \partial_{c_i} n(c_i) (c_i K_C + c_i^2)}{(K_C + c_i)^2} \right)^{-1}, \quad (15)$$

were $K_C = 600 \mu M$, and c_i represents the luminal $[Ca^{2+}]_i^{JSR}$. The total buffering capacity $n(c_i)$ is defined as $n(c_i) = \hat{M}(c_i)n_M + (1 - \hat{M}(c_i))n_D$, where $n_M = 15$ and $n_D = 30$ represent the capacity for monomeric and dimeric CSQ, respectively.⁵⁷

III. SIMULATIONS OF CALCIUM RELEASE EVENT

A. Trigger and stochastic algorithm

In this section, we perform simulations of CREs based on the calcium regulation mechanism described in the preceding section. We examine both spontaneous CREs and LCC-evoked CREs, each initiated by distinct mechanisms.

For spontaneous CREs, RyRs open randomly due to a very small opening probability of RyRs under resting calcium concentrations in physiological conditions or their malfunction in pathological scenarios. The open and close rates are governed by Eq. (2). Under resting conditions, characterized by an approximate $[Ca^{2+}]_i^{SS}$ of $0.1 \mu M$, RyRs predominantly remain closed. An increased ratio between open and closing rates enhances spontaneous RyR openings, leading to the experimental observation of spontaneous sparks.²³ However, these spontaneous sparks are infrequent, making it impractical to comprehensively study CRE behavior using this approach. In our simulations, we employ the rates described in Eq. (2) to mirror realistic conditions, despite yielding negligible sparks at low $[Ca^{2+}]_i^{SS}$. Instead, we initiate spontaneous CREs by briefly placing a RyR in the open state for a duration of 0.001 ms .

The activation of LCCs is a critical trigger for CREs, responding to various stimuli such as changes in voltage, hormonal signals, and signaling molecules. While the dynamics of LCC opening are complex, our focus here is on how LCCs evoke calcium sparks and influence their formation and characteristics. For simplicity, we consider only events with single LCC release; in this case, the formation of a calcium spark is not influenced by multiple LCC releases. Further details will be presented in Section IIIC.

In our study, we utilize a spatial network model where RyRs are considered as nodes within the network. To simulate LCC-evoked CREs, we strategically position LCC calcium release sites in close proximity to RyR nodes, eliminating the need to introduce additional nodes to represent LCCs. The calcium flux is maintained at a constant rate of 0.5 pA , and the duration of LCC opening is consistently set at 6.7 ms , a value derived from the time constant associated with sparklet-spark coupling latency.¹¹ In mode LCC I, only a single LCC release is assigned to a cluster. In mode LCC II, as suggested by experimental observations, LCCs are roughly one-seventh in number compared to the RyRs within a cluster. This configuration ensures the activation of calcium sparks.⁶⁷ Other release type will be also discussed in Section IIIC.

In this study, we employ a stochastic simulation methodology with fixed time steps. At each predetermined interval, for every transition between two of the four states of every RyR, a random number is generated to determine whether the

transition occurs, based on the corresponding transition rates. Simultaneously, calcium concentration is updated in line with the flux dynamics described in the previous section. To ensure accuracy, we use a time step of 0.001 ms, which minimizes the likelihood of multiple reactions occurring within the same time step.

B. Exemplary CREs within a single cluster

In this section, we present examples of spontaneous and LCC-evoked CREs within a cluster consisting of 50 RyRs over a simulation period of 10 s, with triggers occurring every 0.05 s for spontaneous scenarios and every 3 s for LCC-evoked scenarios. The temporal evolution of mean calcium concentrations, $[Ca^{2+}]^{SS}$ and $[Ca^{2+}]^{JSR}$, and the number of open RyRs N_O in the cluster is illustrated in Fig. 5. Additionally, the figure includes a depiction of the spatial structure of the analyzed cluster, generated using the prescribed method.

In the spontaneous scenario, the simulation reveals that most rapidly opening RyRs tend to close soon after and are unable to trigger further opening of other RyRs. Only a few open RyRs can initiate a CRE involving more than one RyR, resulting in short-lived small peaks, characteristic of calcium quarks. Notably, we observe a distinct CRE that induces significant fluctuations in the mean calcium concentration $[Ca^{2+}]^{SS}$ around 5.7 s with open RyRs much more than the calcium quarks. This concentration increases from its resting value of approximately 0.1 μM to around 300 μM . Concurrently, the $[Ca^{2+}]^{JSR}$ decreases from 1 mM to approximately 500 μM , which is consistent with findings in the literature.^{16,17,23–25} Obviously, the Ca^{2+} in JSR is not depleted. LCCs prove highly effective at triggering CREs. In an illustrative simulation [see Fig. 5(c) and (d)], all four LCC triggers evoke CREs with amplitudes similar to those in the spontaneous scenario. These CREs, with long duration and many RyRs involved, align well with experimentally observed spontaneous and LCC-evoked calcium sparks.^{10,11}

The accompanying subfigures offer a detailed representation of the CRE occurring near time $t=5.7$ and 6.0 s for the spontaneous and LCC-evoked scenarios, respectively. Fig. 5(b) illustrates that when a specific RyR is set to the open state, it remains open for roughly 5 ms. During this interval, only this RyR remains open, while the other RyRs stay closed as the $[Ca^{2+}]^{SS}$ increases slowly. After approximately 5 ms, other RyRs are rapidly activated, and the number of open RyRs increases quickly to around 25, representing about half of the total RyRs in the cluster. A similar rapid increase in the number of open RyRs is observed at about 5 ms following LCC release in Fig. 5(d). At the outset of the release, no RyRs are opened, although the $[Ca^{2+}]^{SS}$ increases gradually, akin to the spontaneous case. The LCC release serves a role similar to that of a long-lived open RyR in evoking CREs. The number of open RyRs remains at about 20 and then decreases rapidly within several milliseconds, while the $[Ca^{2+}]^{SS}$ continuously decreases to its resting value. Both of these processes last approximately 20 ms. The time evolution of RyRs and the calcium concentrations in both spontaneous

and LCC-evoked cases exhibit similar behaviors, arising from the shared mechanism post-evocation.

C. CREs on clusters with different sizes

In our preceding discussion, we provided an illustrative example of calcium release within a cluster consisting of 50 RyRs. Triggered by the spontaneous opening of a RyR or LCC calcium release, the cluster functions as an on-off switch, producing calcium quarks with very short lifespans and only a few activated RyRs, or calcium sparks with much longer lifespans and approximately half of the RyRs opened. To gain a broader understanding, we conducted simulations with multiple randomly generated clusters of various sizes, including $N_{RyR} = 30, 50$, and 80.

For the spontaneous scenario, we generated 5000 spatial distributions and their corresponding networks and triggered them 10 times each. As seen in the above examples, LCCs are more effective at evoking calcium sparks. Therefore, we only generated 500 spatial distributions for the LCC-evoked scenario. Additionally, we considered multicenter cases with 1000 RyRs, with 200 and 20 spatial distributions considered for spontaneous and LCC-evoked scenarios, respectively.

In Fig. 6, we present the distribution of the CREs against the peak number of open RyRs, denoted as N_O^{peak} , and the duration of these CREs, represented as τ , for different cluster sizes. As shown in Fig. 5, the activation of a cluster occurs rapidly in the spontaneous scenario, primarily driven by a long-lived RyR channel. To facilitate analysis, we defined the total duration, τ , as the time from the first RyR opening to when all RyRs within the cluster have closed. In the LCC-evoked scenarios, the calcium concentration begins to rise upon LCC opening, marking the onset of the calcium spark. In this case, we defined the initiation time point at the LCC opening to facilitate a direct comparison with spontaneous CREs.

Remarkably, a clear demarcation emerges when distinguishing CREs characterized by peak open RyRs N_O^{peak} and duration τ in both scenarios, as shown in Fig. 6(a-i). To elucidate this, consider the case of an 80 RyR cluster where we can establish a critical threshold at $N_O^{\text{peak}} = 20$ in Fig. 6(a-c). This threshold effectively segregates CREs into two distinct categories. Those above the threshold tend to converge around $N_O^{\text{peak}} = 40$ with a corresponding τ of approximately 25 ms. These larger CREs, characterized by larger N_O^{peak} and τ , are indicative of calcium sparks. They release a more substantial amount of calcium and are more likely to align with experimental observations. Conversely, CREs with smaller N_O^{peak} possess a duration of less than 10 ms with few RyRs, corresponding to calcium quarks. Such results confirm that clusters of RyRs function as on-off switch.

The 2D histogram shown in Fig. 6(a, d, g) for the spontaneous CREs exhibits a similar shape to the histograms in Fig. 6 (b, e, h) for LCC-evoked CREs with initiation mode I. It is consistent with the observed similarity of the two types of calcium sparks in experiments.¹¹ Moreover, LCC release is much more effective at evoking CREs than rapidly opening

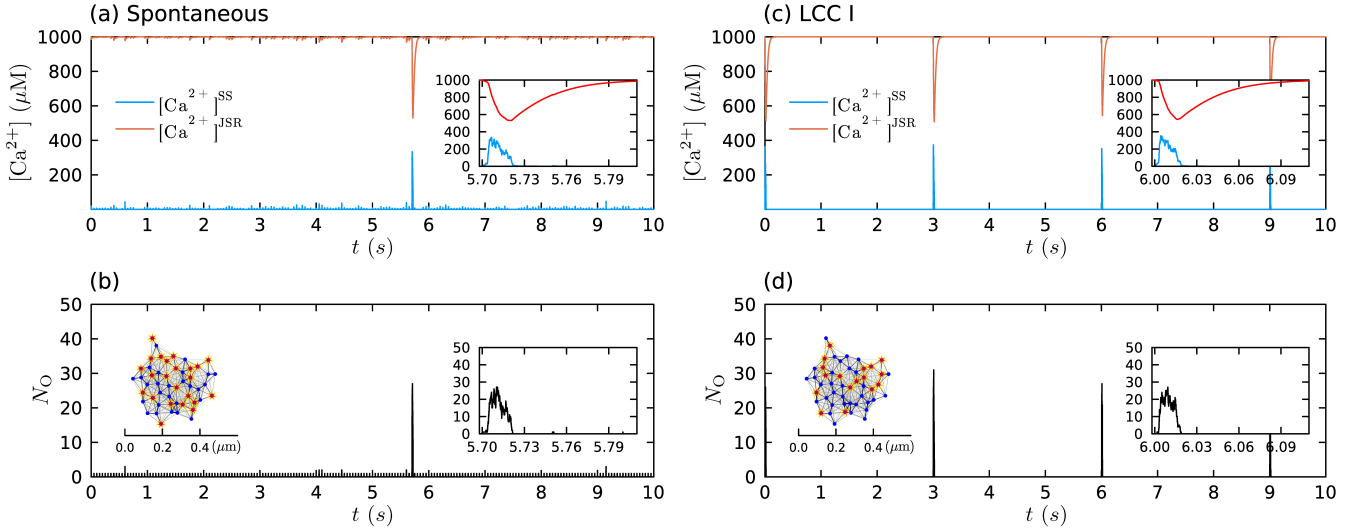


FIG. 5. Temporal calcium release profile in a single cluster of 50 RyRs for the spontaneous scenario (panels a, b) and LCC I scenario (panels c, d). (a, c) Depicts the temporal evolution of mean calcium concentrations, including $[Ca^{2+}]^{SS}$ (blue curves) and $[Ca^{2+}]^{JSR}$ (red curves). (b, d) show the variation in the number of open RyR channels N_O over time. The right subfigure highlights the CREs near $t = 5.7$ and 6.0 s for the spontaneous (a, b) and LCC I (c, d) scenarios, respectively. The subfigure on the left illustrates the spatial network of the analyzed cluster with opened RyRs (red stars with yellow borders) at 5.71 and 6.01 s for spontaneous and LCC I scenarios, respectively.

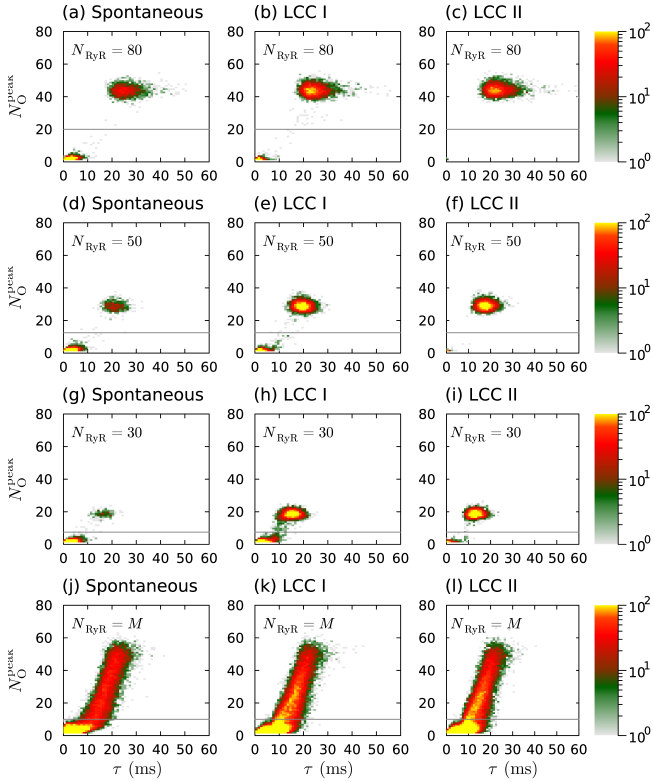


FIG. 6. 2D histograms representing the distribution of CREs on clusters with sizes 80, 30, and 50, as well as multicluster cases (M), against the number of peak open RyRs N_O^{peak} and duration τ , with bin sizes of 1 and 1 ms, respectively. Horizontal lines in panels (a-i) and panels (j-l) indicate N_O^{peak} values of $N_{\text{RyR}}/4$ and 10, respectively.

RyRs. As depicted in Fig. 6, the number of CREs in the LCC-evoked scenario I, even with fewer triggers, is significantly larger than in the spontaneous case. We also adopted mode II in the LCC-evoked scenario, which aligns with experimental findings suggesting that LCCs number approximately 1/7 of the RyRs within a cluster, ensuring the activation of calcium sparks.⁶⁷

To provide a clearer understanding of the properties of CREs with respect to cluster size, we also present reference results with multicluster configurations in Fig. 6(j-l). In the current work, the cluster size obeys a power-law distribution following the experimental results.^{33–35,60,61} The frequency of clusters with a size larger than 10 is smaller and decreases slower than those with a size smaller than 10. The results suggest that the time scale of CREs for different cluster size is about 20 ms, while N_O^{peak} has a wide spread from 0 to about 50. When combined with the results from a single cluster, it is evident that the amplitudes of calcium sparks are determined by the cluster size, while the duration is less sensitive to the cluster size.

D. Calcium sparks with different LCC triggers

In this work, we consider triggers with a single release from LCCs as a constant calcium flux to evoke calcium sparks. However, the opening dynamics of LCCs are much more complex. For instance, LCCs typically have multiple states and transition between them, and several detailed mechanisms have been developed to describe LCC opening and the corresponding calcium flux.^{50,53,68–71} Our focus here is on how LCCs evoke calcium sparks and the formation and characteristics of these sparks. Therefore, we only consider events with

a single LCC release. In this case, the formation of a calcium spark is not influenced by multiple LCC releases. This approach is reasonable for in vitro experiments studying the formation and properties of individual calcium sparks and is also applicable to some physiological conditions, as well as certain pathological scenarios.

Typically, during LCC opening and calcium release, the calcium flux is treated as constant.^{16,17} However, the duration and magnitude of this flux can vary. For example, as noted in previous studies, the opening duration of LCCs can range from approximately 0.1 ms to around 20 ms.¹¹ Here, we will discuss whether such differences in opening time and flux constant of LCC affect the formation and characteristics of calcium sparks. The results of this analysis with a cluster of 50 RyRs as example are presented in Fig. 7.

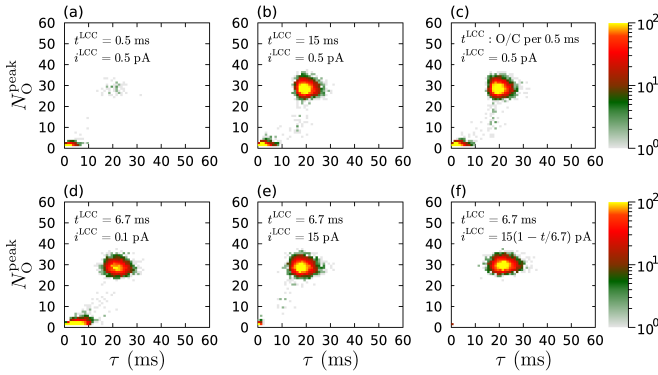


FIG. 7. 2D histograms representing the distribution of CREs on clusters of size 50 with different LCC triggers. Pannels (a), (b), and (c) show a constant flux $i_{LCC}^0 = 0.5$ pA with durations t_{LCC}^0 of 0.5 ms, 15 ms, and an interval of opening and closing every 0.5 ms over a total period of 15 ms, respectively. Pannels (d), (e), and (f) show a fixed LCC duration of 6.7 ms, with varying flux strengths: $i_{LCC}^0 = 0.1$ pA, $i_{LCC}^0 = 15$ pA, and $i_{LCC}^0 = 15(1 - t/6.7)$ pA, respectively.

In the calculations in above sections, we considered an LCC release with a flux constant of $i_{LCC}^0 = 0.5$ pA and a duration of 6.7 ms. Here, we keep the flux constant at 0.5 pA and varied the duration to 0.5 ms, which is typical of LCC opening times under physiological conditions, and to 15 ms, a longer duration observed under experimental conditions,¹¹ as shown in Fig. 7 (a) and (b). Additionally, we examined a case where the LCC opened and closed at intervals of 0.5 ms over a total period of 15 ms, as presented in Fig. 7 (c). The results show that longer LCC durations increase the occurrence of calcium sparks, while the peak number of open RyRs N_O^{peak} and the duration τ of the calcium sparks remain largely unaffected by the LCC duration.

In Fig. 7 (d-f), we keep the duration time of LCC fixed at 6.7 ms and vary the flux constant, considering cases with $i_{LCC}^0 = 0.1$ pA and $i_{LCC}^0 = 15$ pA, as well as a linearly decreasing flux modeled as $i_{LCC}^0 = 15(1 - t/6.7)$ pA. The results indicate that increasing the flux strength significantly raises the likelihood of calcium spark initiation. However, despite this increase in spark probability, the general properties of the calcium sparks, such as their duration and amplitude, remain

consistent across different flux strengths.

These results suggest that if a calcium spark is triggered by a single release from LCCs, its properties remain largely independent of the specific trigger type. The differences in the type of trigger mainly influence the likelihood of calcium spark occurrence. Thus, the explicit mechanisms governing LCC state transitions impact the general scale of RyR release and, consequently, the overall calcium release within the cell. However, in this study, we focus solely on the probabilities associated with individual calcium sparks. Therefore, in the following calculations, we consider only an LCC release with a constant flux of $i_{LCC}^0 = 0.5$ pA and a duration of 6.7 ms.

IV. REGULATION OF CLACIUM SPARKS

In previous sections, we explored the formation of calcium sparks and observed that their peak number of open RyRs and duration remain consistent, whether evoked spontaneously or triggered by various types of LCC release. In this section, we examine the regulation of calcium sparks by analyzing the influence of RyR transition rates, calcium concentrations in the NSR and myoplasm, and the role of CSQ.

A. Regulation by RyR transition rates

Cannell et al. highlighted significant differences in RyR behavior between rats and sheep.²³ As illustrated in Fig. 3, the transition rates of RyRs differ between species. While it is clear that the magnitude of the RyR transition rate influences the likelihood of calcium spark occurrence, the question remains: does it also impact the characteristics of the calcium sparks themselves? To explore this, we present in Fig. 8 the results using different transition rates with 10000 simulations under a LCC trigger, investigating their potential effects on calcium spark properties.

In Fig. 8 (a), we present the results using the transition rates for rat RyRs as fitted by Cannell et al., shown as the dotted line in Fig. 3. These rates have been applied in the previous calculations. The results show a clear concentration of CREs. When the transition rates are adjusted to those fitted using the sigmoid form for the opening rate and a constant closing rate, the calcium spark properties, including the peak number of open RyRs N_O^{peak} and spark duration τ , remain largely unchanged. This is expected due to the similarity between the two fitting approaches. When the value of K in the sigmoid form of the opening rate is halved, the peak number of open RyRs N_O^{peak} remains nearly constant, while some calcium sparks exhibit longer durations. This aligns with the open probability results in Fig. 3(c), where a reduction in K increases the open probability of RyRs.

The results for sheep, using the transition rates fitted by Cannell et al., are shown in Fig. 8(d). These results indicate a higher occurrence of calcium sparks with longer durations, which is attributed to the larger opening rates and smaller closing rates for RyRs in sheep, particularly the continuous decrease in the closing rate as calcium concentration increases.

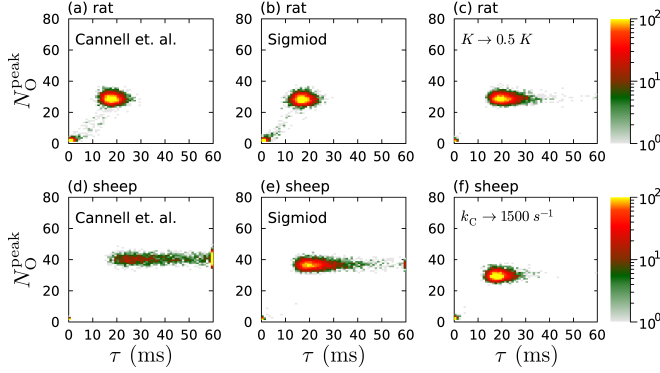


FIG. 8. 2D histograms representing the distribution of CREs on clusters of size 50 with varying RyR transition rates. (a) Transition rates for rat RyRs as fitted by Cannell et al. (b) Transition rates for rat RyRs fitted using the sigmoid form. (c) Same as (b) but with K reduced to $0.5K$. (d) Transition rates for sheep RyRs as fitted by Cannell et al. (e) Transition rates for sheep RyRs fitted using the sigmoid form. (f) Same as (e) but with the closing rate increased to 1500 s^{-1} .

When we use the sigmoid form for the transition rates, the number of calcium sparks with longer duration decreases significantly, as shown in Fig. 8(e). Further increasing the closing rate from 810.0 s^{-1} to 1500 s^{-1} leads to an additional reduction in calcium sparks with longer duration, bringing the results closer to those seen in rats.

To further understand the regulation of calcium sparks through variations in the RyR opening rate, we present in Fig. 9 the results of spontaneous calcium sparks with different RyR opening rates, normalized to the opening rate of rats. The results indicate that the number of calcium sparks increases rapidly with higher opening rates. Similarly, the peak number of open RyRs also rises quickly as the opening rate increases, although this increase slows at higher open rates. Surprisingly, the effect on spark duration is minimal; after a slight decrease, the duration stabilizes at around 20 ms. These findings suggest that increasing the RyR opening rate enhances calcium release through calcium sparks by increasing both the number of calcium sparks and the number of RyRs activated within a cluster, while having little impact on spark duration.

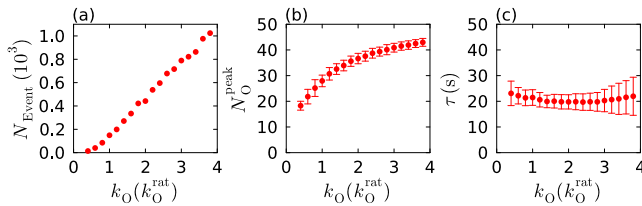


FIG. 9. Number of calcium sparks (a), peak number of open RyR (b), and duration (c) of calcium sparks in clusters of size 50, with varying RyR opening rates, expressed as multiples of the experimentally measured opening rate for rat RyRs.

With the results presented in Fig. 9, at the experimental opening rate, approximately 100 spontaneous calcium sparks occur for every 10,000 openings of RyR channels. Consider-

ing the estimated number of RyRs in a cell, which is on the order of 10^6 as reported by Cheng et al.,¹⁰ if the probability of spontaneous openings of RyR is 1%, the experimental observations of approximately 100 calcium sparks can indeed be achieved.¹⁰

B. Regulation by calcium concentrations in NSR and myoplasm

In the current study, we investigate calcium release with calcium concentrations in the JSR and myoplasm clamped. However, in vivo environments, these calcium concentrations will vary due to calcium release or other reasons. Now, we discuss the effect of these calcium concentrations on calcium release. In Fig. 10, we present the distribution of N_O^{peak} and τ with different calcium concentrations in the JSR and myoplasm. In the simulation, 200 partial distributions of a single cluster with 50 RyRs are generated, and 10 triggers are performed with time evolution lasting 100 ms (all CREs with τ larger than 100 ms will be categorized to 100 ms).

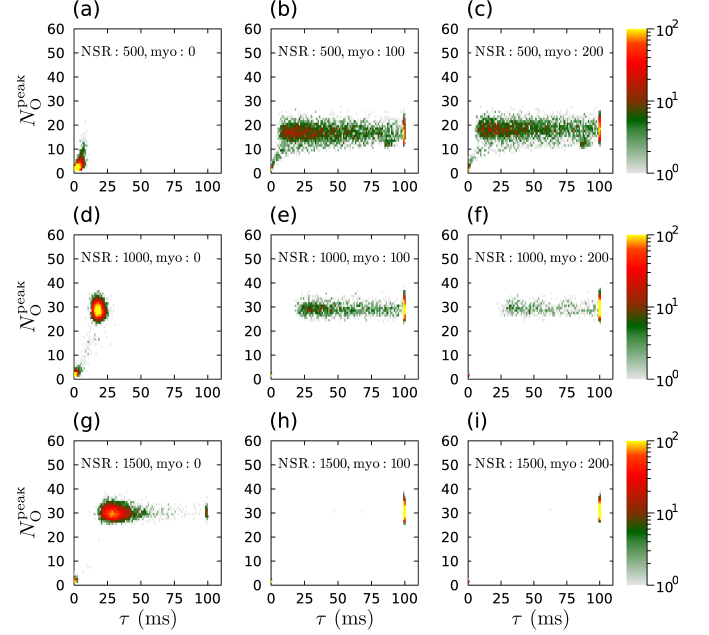


FIG. 10. 2D histogram representing the distribution of CREs on clusters with size 50 against the number of peak open RyRs N_O^{peak} and duration τ . The distributions are shown for different levels of calcium concentrations: $500 \mu\text{M}$ (a, b, c), $1000 \mu\text{M}$ (d, e, f), and $1500 \mu\text{M}$ (g, h, i) in NSR, and $0 \mu\text{M}$ (a, d, g), $100 \mu\text{M}$ (b, e, h), and $200 \mu\text{M}$ (c, f, i) in the myoplasm. The bin sizes for N_O^{peak} and τ are 1 and 1 ms, respectively.

For the low calcium concentration in myoplasm, chosen as $0 \mu\text{M}$ in simulation, calcium sparks are difficult to evoke if $[\text{Ca}^{2+}]^{\text{NSR}}$ is set as $500 \mu\text{M}$. As shown in Fig. 10(a), most of the CREs have N_O^{peak} smaller than 10 and τ smaller than 10. With the increase of $[\text{Ca}^{2+}]^{\text{NSR}}$, larger calcium sparks are evoked. The N_O^{peak} is kept at about 30 and changes lit-

tle with the $[Ca^{2+}]^{NSR}$ ranging from $1000 \mu M$ to $1500 \mu M$, while the duration τ lasts longer. With high $[Ca^{2+}]^{NSR}$, the calcium sparks with long lifetimes become more frequent, and some of them even have a duration of more than 100 ms with $[Ca^{2+}]^{NSR}$ of $1500 \mu M$. The high calcium concentration in NSR may lead to a high calcium concentration in JSR $[Ca^{2+}]^{JSR}$, resulting in larger calcium releases from the JSR to SS, which could be the reason for the longer duration.

For larger calcium concentrations in myoplasm, $[Ca^{2+}]^{myo}$ of $100 \mu M$ and $200 \mu M$, which will lead to a high calcium concentration in SS $[Ca^{2+}]^{SS}$. The sensitivity of the RyR is dependent on $[Ca^{2+}]^{SS}$; hence, calcium release is easier to occur and sustain. For $[Ca^{2+}]^{NSR}$ set as $500 \mu M$, the calcium sparks occur with smaller amplitudes, N_O^{peak} about 20, and the duration has a sparse distribution, ranging from smaller than 10 ms to larger than 100 ms. With the increase of $[Ca^{2+}]^{NSR}$, the amplitudes become larger and stabilize around 30. The durations become longer, and most of them are larger than 100 ms at $[Ca^{2+}]^{NSR}$ of $1500 \mu M$.

To further understand the regulation of calcium sparks under varying calcium concentrations in the NSR and myoplasm, we present the results of spontaneous calcium sparks under different calcium levels in Fig. 11. As the calcium concentration in the NSR increases, the frequency of spontaneous calcium sparks rises, as shown in Fig. 11(a). However, the peak number of open RyRs N_O^{peak} remains mostly stable, with only a slight increase at lower concentrations, while the duration time decreases gradually. In Fig. 11(c), we also provide results of Sato et al.,⁵⁶ showing consistency between our findings and theirs, both in terms of the duration times and the trend as $[Ca^{2+}]^{NSR}$ increases. Additionally, the results in Fig. 11(a-c) suggest a rapid increase in flux rate at $[Ca^{2+}]^{NSR}$ levels around $600 \mu M$, which aligns with the findings of Sato et al.⁵⁵

Increasing the calcium concentration in the myoplasm causes a rapid rise in the number of calcium sparks, reaching 10,000, which corresponds to the total number of triggers. This indicates that nearly all spontaneous openings of RyRs trigger calcium sparks. Despite this, the increase in myoplasmic calcium concentration has little effect on the peak number of open RyRs N_O^{peak} , which stabilizes around 30. The duration of calcium sparks remains stable at lower concentrations but increases sharply with higher concentrations. Though the duration appears to stabilize again, as shown in Fig. 11(f), this is mainly due to the calculation being limited to 60 ms.

These findings suggest that increasing calcium concentrations in both the NSR and myoplasm primarily enhances calcium release through calcium sparks by increasing the number of sparks and their duration, with minimal effect on the number of RyRs activated within a cluster.

C. Regulation by Calsequestrin

The CSQ serves as a critical regulator of calcium release. Its binding and unbinding from the RyR complex influence the sensitivity of RyRs to calcium. Additionally, CSQ can bind calcium ions in the JSR, thereby regulating the calcium

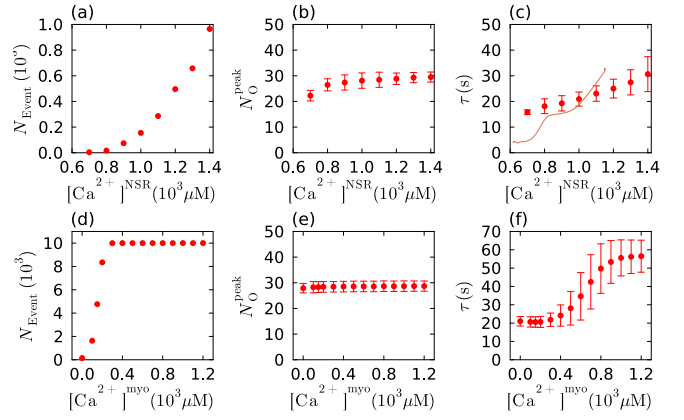


FIG. 11. Number of calcium sparks (a, d), peak number of open RyRs (b, e), and duration (c, f) of calcium sparks in clusters of size 50, with varying calcium concentrations in the NSR (a, b, c) and myoplasm (d, e, f). The line in (c) is restuls by Sato et al.⁵⁶

concentration within this compartment. In our model, we introduce binding and unbinding states to simulate the fluctuating sensitivity of RyRs to CSQ as shown in Fig. 2, while a β factor represents the buffering effect of CSQ in Eq. (1) and Eq. (15).

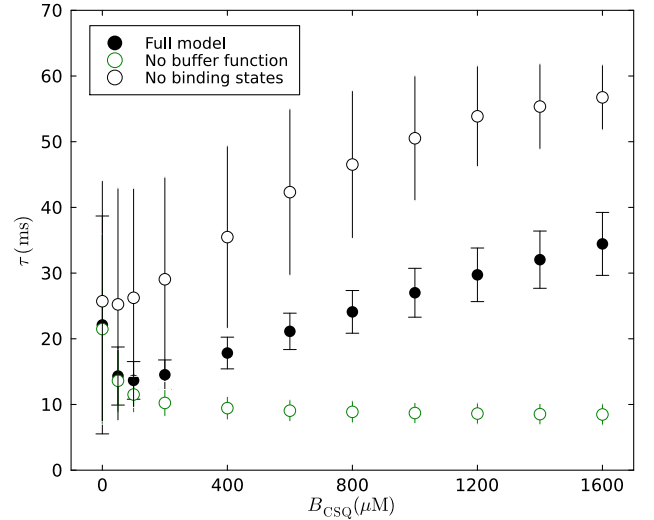


FIG. 12. Variation of the duration of calcium sparks with CSQ concentration B_{CSQ} . The black solid circles represent the results from the full model, while the green open circles and black open circles represent models without the buffer function of CSQ and without the two CSQ binding states, respectively.

Fig. 12 illustrates the variation of durations of CREs corresponding to changes in CSQ concentration. The results obtained with a CSQ concentration of $0 \mu M$ exhibit a widely spread distribution of calcium release events across the duration τ . As the CSQ concentration increases, this distribution narrows, indicating a more stable duration for clusters of certain size. Increasing CSQ levels prolong the calcium release duration from approximately 10 ms with $100 \mu M$ to 30 ms

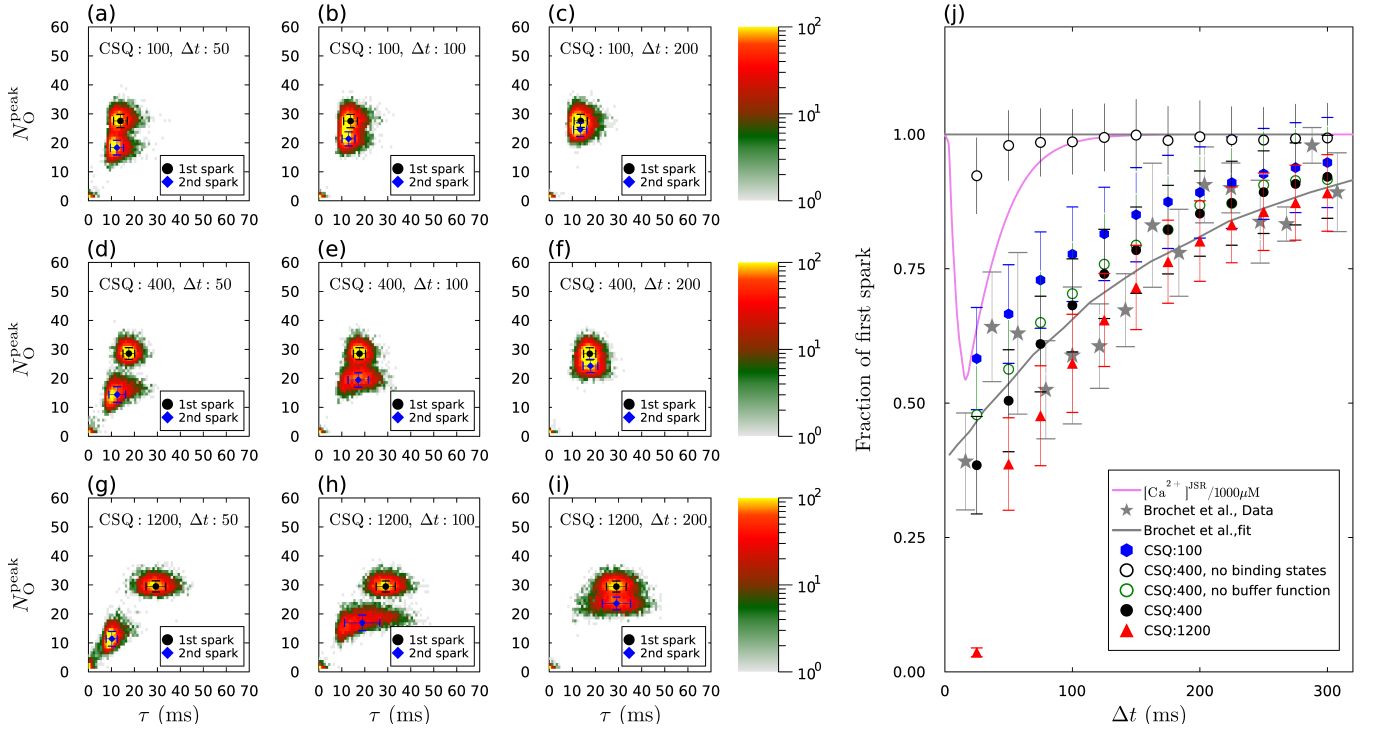


FIG. 13. Refractoriness of the calcium sparks with different interval times Δt . (a-i) 2D histogram depicting the distribution of N_O^{peak} and τ with different CSQ concentrations and interval times Δt . The bin sizes for N_O^{peak} and τ are 1 and 1 ms, respectively. The black circle and blue diamond represent the average and uncertainties of N_O^{peak} and τ for the first and second sparks. (j) The N_O^{peak} of the second spark as the fraction of the first spark. The blue hexagon, black full (black empty, green empty) circle, and red triangle represent the CSQ concentrations of 100, 400 (without binding state, without buffer function), 1200 μM . The solid curves depict a typical normalized JSR depletion curve, $[\text{Ca}^{2+}]^{\text{JSR}}/100 \mu\text{M}$, showing that the recovery from refractoriness is not associated with local JSR refilling. Experimental results and fitting (grey star and curve) from Brochet et al.⁵¹

with 1600 μM . CSQ plays a dual role in regulating calcium release: affecting the sensitivity of RyRs to calcium and serving as a buffer to sequester calcium in the JSR. To elucidate the origin of the duration variation, we also provide results without the β factor in Eq. (1), which removes the buffer function, as the green open circles in Fig. 12. In this case, the duration remains largely unchanged with increasing CSQ concentration. However, if we maintain the buffer function but remove the binding state, the prolongation of duration can still be observed as shown as black open circles in Fig. 12. This verifies that the variation in duration is primarily due to the buffering action of CSQ inside the SR, as suggested by Terentyev et al.⁴⁰

As depicted in Fig. 5, a calcium spark lasts approximately 20 ms, after which the RyRs close and the calcium concentration in the SS returns to its resting state. However, the calcium blink in the JSR persists longer after the RyR closure and termination of the calcium sparks in the SS. During this period, the calcium concentration in the JSR $[\text{Ca}^{2+}]^{\text{JSR}}$ does not fully recover to 1000 μM , reducing the likelihood of subsequent calcium sparks. As simulated in our study and by other researchers, the calcium blink typically occurs on a timescale of about 100 ms. Interestingly, experimental measurements of refractoriness are often much longer than those derived from the calcium blink.⁵¹ Such excess refractoriness may result

from the CSQ affecting the activity of RyRs. In our model, the regulation of RyRs by CSQ is accomplished through two binding states, as described by Restrepo et al.⁵⁰ Here, we present our findings regarding refractoriness in Fig. 13.

In the simulation, the RyRs are activated by LCC calcium release in model II scenario, wherein a cluster of 50 RyRs is paired with 50/7 LCCs. Such activations ensure that a calcium spark can be evoked with a trigger. After an interval Δt following the termination of the first calcium spark, another activation is performed to trigger the second calcium spark. We generate 500 partial distributions of the cluster, and for each distribution, 10 simulations are performed. The N_O^{peak} and τ of calcium sparks are collected.

In Fig. 13(a-i), two groups of CREs are evident. The group with larger N_O^{peak} corresponds to the first sparks, while the other with smaller N_O^{peak} represents the second sparks. Comparing the subfigures for the same CSQ concentration, one can observe that with increasing intervals, the two groups gradually merge into one, indicating the disappearance of refractoriness. Moreover, as the CSQ concentration increases, the deviation of the second spark from the first sparks becomes larger.

The N_O^{peak} of the second spark as the fraction of the first spark is shown in Fig. 13(j) and compared with changes in

calcium concentration in the JSR as well as experimental results. This figure illustrates that at high levels of CSQ concentration, the fraction of first sparks resulting in second sparks becomes smaller, consistent with findings by Restrepo et al.⁵⁰ Our model reproduces these observed properties, aligning with the experimental findings of Terentyev et al.,⁴⁰ which demonstrate that the refractory period increases when CSQ is overexpressed in transgenic mice. To confirm that the increased spark refractoriness is not caused by the refilling of local JSR stores, we plot a typical JSR depletion curve, i.e., $[Ca^{2+}]^{SS}/100 \mu M$, as a function of time. As shown in the figure, the JSR stores refill much faster than the time it takes for the second spark to reach the same level as the first spark. This indicates that factors beyond simple ion replenishment are contributing to the refractory period.

To investigate the origins of the excess refractoriness, we also provide results with the removal of the β factor and the binding state. These results differ significantly from the variation of duration with CSQ concentration described above. Without the buffer function, the fraction remains almost the same as in the full model. However, if we retain the buffer function but remove the binding state, the excess refractoriness vanishes, and the fractions increase to 1 as $[Ca^{2+}]^{SS}/100 \mu M$. These findings suggest that the excess refractoriness is primarily due to the CSQ-dependent sensitivity of the RyR, rather than the buffering action of this protein inside the JSR. The CSQ binding state appears to play a crucial role in modulating RyR activity, leading to prolonged refractory periods. When the CSQ binding state is removed, RyRs regain their normal sensitivity more quickly, resulting in a faster recovery and a higher likelihood of subsequent sparks occurring at a similar magnitude to the initial spark.

D. CREs under malfunctioning calsequestrin regulation

The simulations presented above suggest that the CSQ has a dual role in regulating calcium release. If the CSQ regulation mechanism malfunctions, the calcium release becomes irregular. Here, we investigate two malfunctioning scenarios that result in a decrease in calcium release: CSQ release dysfunction from the RyR complex, as shown in Fig. 14(a-c), and malfunction of the buffering function of CSQ, as depicted in Fig. 14(d-f). During the simulations, 500 partial distributions of a cluster comprising 50 RyRs were generated, and 10 triggers were applied with a time evolution of 100 ms (all CREs with τ values greater than 100 ms were categorized as having a duration of 100 ms).

In Fig. 14(a-d), the calcium concentrations in the NSR and myoplasm are set to standard values of 1000 and $0.1 \mu M$, respectively. When the RyR complex is bound with CSQ, it exhibits low activity and is less likely to open. If the CSQ malfunctions when releasing from the RyR complex, the RyR becomes harder to open, resulting in very short-duration CREs and few open RyRs, as seen in Fig. 14(a). On the other hand, if the CSQ cannot buffer calcium in the JSR, a significant number of RyRs within a cluster still open, but with a short duration, as shown in Fig. 14(b). Both of these malfunctions in

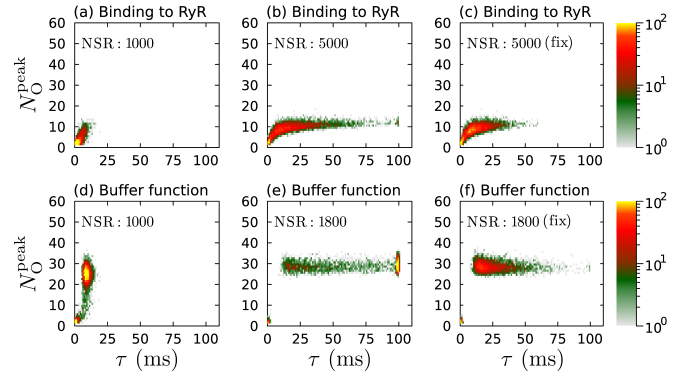


FIG. 14. 2D histogram representing the distribution of CREs under CSQ malfunction conditions. Panels (a-c) illustrate the scenario where all RyR are bound by CSQ, while panels (d-f) depict a malfunction in the buffering function of CSQ. Panels (a,d), (b,e), and (c,f) correspond to $[Ca^{2+}]^{NSR}$ concentrations of 1000 and 5000 (1800) μM for different spatial distributions of RyR clusters, and 5000 (1800) μM for a fixed spatial distribution, respectively.

CSQ regulation reduce calcium release from the JSR. To increase calcium release, the $[Ca^{2+}]^{NSR}$ was increased to 5000 and 1800 μM in two scenarios, respectively. This indeed enhanced calcium release in both scenarios [Fig. 14(b,e)]. However, one can observe that the distribution of CRE durations becomes more dispersed, indicating that the on-off switch characteristics of cluster cannot be fully recovered to those observed with standard $[Ca^{2+}]^{NSR}$ value. To further investigate whether this dispersion is due to differences in spatial distribution, we fixed the spatial distribution of the RyR cluster and performed 5000 triggers. As seen in Fig. 14(c, f), the results still exhibit dispersion, indicating that the on-off switching characteristic of a RyR cluster is not fully restored for a RyR cluster, even with increased calcium release.

V. DISCUSSION AND SUMMARY

The RyRs form clusters that exhibit irregular shapes, varying sizes, and a stochastic distribution of receptors. In the current study, we have depicted the spatial distribution of RyRs using a nonlinear spatial network. By integrating calcium exchange mechanisms and calcium buffering dynamics, we have successfully constructed a model that simulates calcium release through RyRs located on the JSR under conditions of clamped calcium concentrations in the NSR and myoplasm.

A. RyR Cluster On-Off Behavior

Our model successfully reproduces the characteristic on-off behavior of RyR clusters during calcium release. In spontaneous simulation scenarios, RyRs open briefly for approximately 0.001ms, with only a few remaining open for over 1ms, potentially triggering CREs. These CREs can be classified into two categories: short-lived calcium quarks, lasting

less than 10ms with only a few activated RyRs, and longer-lasting calcium sparks, involving significantly more RyRs. These findings confirm that RyR clusters operate as on-off switches in calcium release, as suggested by prior studies.^{8,9} While the probability of initiating a calcium spark from random RyR openings is low, our simulations show that sustained LCC release for 6.7ms can reliably trigger calcium sparks. These sparks exhibit similar characteristics to spontaneous sparks in terms of duration and other key properties, consistent with experimental observations.^{10–12} Notably, this behavior is robust across various LCC triggers, further validating the model's predictive capabilities.

Mechanisms Governing Spark Termination: The duration of calcium sparks is determined primarily by their termination mechanisms, which have been widely studied in the literature. Proposed explanations include local calcium depletion in JSR and "stochastic attrition".^{72–74} In our model, spark termination is governed by the reduction of the calcium gradient between the subspace and JSR, as well as the stochastic opening and closing of RyRs. This suggests that termination is not solely dependent on complete JSR depletion or stochastic attrition. During a calcium spark, the calcium concentration in the JSR decreases but stabilizes at approximately 500 μM . Interestingly, when the JSR calcium concentration falls below 500 μM , CSQ begins to bind to RyRs, reducing RyR activity and facilitating spark termination. This mechanism highlights the role of CSQ in modulating calcium release dynamics.

Modulation by Species-Specific RyR Properties: Cannell et al. revealed notable differences in RyR behavior between rats and sheep, particularly in the transition rates affecting CREs.²³ For rat RyRs, both the transition rates used in the original study and a newly proposed sigmoid fit show a concentration of CREs. However, reducing the RyR opening rate parameter can extend spark durations in certain cases. In contrast, for sheep RyRs, the transition rates suggested by Cannell et al.²³ result in longer calcium sparks due to a continuous decrease in the closing rate with increasing calcium concentration, which appears unrealistic. By adjusting to a constant closing rate in the new sigmoid fit, the results align more closely with observations in rats. Furthermore, variations in RyR opening rates increase the number of calcium sparks and activated RyRs with minimal impact on spark duration, suggesting that increased RyR opening primarily facilitates calcium release.

Calcium Concentration Effects on CRE Dynamics: The resting myoplasmic calcium concentration is approximately 0.1 μM , which is critical for maintaining stable calcium sparks with a duration of around 20 ms. When the myoplasmic calcium concentration is increased to 100 μM , the distribution of spark durations becomes sparse, with some lasting over 100 ms. Higher calcium concentrations in both the myoplasm and the NSR are necessary to effectively reproduce calcium sparks. Lower NSR calcium concentrations result in CREs with short durations or sparse distributions, while higher NSR calcium concentrations lead to significantly prolonged CREs. Additionally, increased calcium release elevates myoplasmic calcium levels, further prolonging CRE du-

rations and potentially triggering intracellular calcium oscillations. These findings suggest that elevating calcium concentrations in the NSR and myoplasm enhances calcium release by increasing the number and duration of calcium sparks, with minimal impact on the number of RyRs activated within a cluster.

B. CSQ as a Key Modulator of Calcium Release

The intricate role of CSQ in calcium release regulation is critical for understanding the pathophysiology of various diseases.^{43,48,49} This study investigates two key mechanisms through which CSQ influences calcium dynamics: its role as a calcium buffer within the JSR and its interaction with RyRs to modulate their activity. Using computational simulations, we examined the effects of varying CSQ concentrations on CRE durations and the phenomenon of excess refractoriness.

CSQ as a Buffer: Our results confirm the dual role of CSQ in calcium regulation, consistent with prior studies.^{41–43} Specifically, variations in CSQ concentrations significantly influence CRE durations, in agreement with experimental observations.⁴⁰ By selectively removing CSQ's buffering function and its binding interactions, we found that its primary influence on CRE durations arises from its buffering capacity in the JSR. This underscores the pivotal role of CSQ in shaping the temporal profile of calcium release by maintaining calcium homeostasis within the JSR.

CSQ-RyR Interaction: In addition to its buffering role, CSQ interacts with RyRs to regulate their activity and sensitivity, a mechanism closely tied to excess refractoriness observed experimentally.⁵¹ Our simulations demonstrate that removing CSQ-RyR binding states led to a significant reduction in refractory periods. This indicates that the interaction between CSQ and RyRs is critical for modulating RyR sensitivity and regulating calcium release dynamics. These findings highlight the complex interplay between CSQ and RyRs in stabilizing calcium signaling within cardiomyocytes.

Impacts of CSQ Dysregulation: Further analysis revealed the impact of CSQ dysregulation on calcium release dynamics. Excessive binding of CSQ to RyRs, coupled with the loss of its buffering function, impeded the proper opening of RyRs. While an increase in NSR calcium concentrations partially restored calcium release, the durations of calcium sparks exhibited a broad range of variability. More importantly, the characteristic on-off switching behavior of RyR clusters was not restored under these conditions. This indicates that CSQ dysregulation disrupts calcium release dynamics and undermines the functional integrity of RyR clusters.

C. Conclusions and Future Perspectives

This study highlights the critical role of RyR clusters in calcium release, emphasizing their robust on-off switch behavior. This switching mechanism forms the foundation of calcium dynamics, with CSQ serving as a key modulator that influences the temporal and spatial characteristics of calcium re-

lease through its buffering capacity and interaction with RyRs. Dysregulation of CSQ functions leads to significant disruptions in calcium signaling, shedding light on its potential involvement in the pathophysiology of cardiac diseases.

Our findings demonstrate that, under calcium-clamped conditions with a realistic RyR2 network, RyR clusters exhibit robust spark structures of varying sizes and achieve switch-like behavior without requiring inactivation mechanisms. These results underscore the importance of network realism in facilitating the emergence of switch-type behavior in RyR clusters.

While this study provides valuable insights, it is important to acknowledge that the calcium-clamped setup represents a simplified system. Future research should extend these findings by exploring RyR dynamics under more physiologically relevant cycling conditions, where calcium concentrations fluctuate continuously. Investigating the interplay between RyR clusters and CSQ in such dynamic scenarios will be crucial for fully understanding calcium signaling mechanisms in cardiomyocytes.

Moreover, future studies should focus on whether the robust switch-type behavior observed here can be sustained under real cycling conditions, and on the specific roles CSQ plays in modulating RyR cluster activity in such systems. By addressing these questions, we can deepen our understanding of RyR-mediated calcium release and develop more comprehensive models of calcium signaling in health and disease.

ACKNOWLEDGMENTS

This project is supported by the National Natural Science Foundation of China (Grant No. 12475080, 11675228).

DATA AVAILABILITY STATEMENT

The data that support the findings of this study are available within the article as well as from the corresponding author upon reasonable request.

- ¹X. H. T. Wehrens, S. E. Lehnart, and A. R. Marks, "Intracellular calcium release and cardiac disease," *Annual Review of Physiology* **67**, 69–98 (2005).
- ²H. Cheng and W. J. Lederer, "Calcium sparks," *Physiological Reviews* **88**, 1491 (2008).
- ³D. Terentyev, I. Györke, A. E. Belevych, and et al., "Redox modification of ryanodine receptors contributes to sarcoplasmic reticulum Ca^{2+} leak in chronic heart failure," *Circulation Research* **103**, 1466–1472 (2008).
- ⁴M. Endo, "Calcium-induced calcium release in skeletal muscle," *Physiological Reviews* **89**, 1153–1176 (2009).
- ⁵D. M. Bers, "Cardiac sarcoplasmic reticulum calcium leak: basis and roles in cardiac dysfunction," *Annual Review of Physiology* **76**, 107 (2013).
- ⁶M. J. Berridge, "The inositol trisphosphate/calcium signaling pathway in health and disease," *Physiological Reviews* **96**, 1261–1296 (2016).
- ⁷D. A. Eisner, J. L. Caldwell, K. Kistamás, and A. W. Trafford, "Calcium and excitation-contraction coupling in the heart," *Circulation Research* **121**, 181 (2017).
- ⁸M. Asfaw, E. Alvarez-Lacalle, and Y. Shiferaw, "The timing statistics of spontaneous calcium release in cardiac myocytes," *PLoS ONE* **8**, e62967 (2013).
- ⁹Z. Song, A. Karma, J. N. Weiss, and Z. Qu, "Long-lasting sparks: Multi-metastability and release competition in the calcium release unit network," *PLoS Computational Biology* **12**, e1004671 (2016).

- ¹⁰H. Cheng, W. J. Lederer, and M. B. Cannell, "Calcium sparks: Elementary events underlying excitation-contraction coupling in heart muscle," *Science* **262**, 740–744 (1993).
- ¹¹S. Q. Wang, L. S. Song, E. G. Lakatta, and H. Cheng, " Ca^{2+} signalling between single l-type Ca^{2+} channels and ryanodine receptors in heart cells," *Nature* **410**, 592–596 (2001).
- ¹²J. R. Lopez-Lopez, P. Shacklock, C. Balke, and W. Wier, "Local calcium transients triggered by single l-type calcium channel currents in cardiac cells," *Science* **268**, 1042–1045 (1995).
- ¹³D. M. Bers, "Cardiac excitation-contraction coupling," *Nature* **415**, 198–205 (2002).
- ¹⁴W. N. Ross, "Understanding calcium waves and sparks in central neurons," *Nature Reviews Neuroscience* **13**, 157–168 (2012).
- ¹⁵S. Feske, "Calcium signalling in lymphocyte activation and disease," *Nature Reviews Immunology* **7**, 690 (2007).
- ¹⁶E. A. Sobie, K. W. Dilly, J. dos Santos Cruz, W. J. Lederer, and M. S. Jafri, "Termination of cardiac Ca^{2+} sparks: An investigative mathematical model of calcium-induced calcium release," *Biophysical Journal* **83**, 59–78 (2002).
- ¹⁷G. B. Williams, A. Chikando, H.-T. M. Tuan, E. Sobie, W. J. Lederer, and M. S. Jafri, "Dynamics of calcium sparks and calcium leak in the heart," *Biophysical Journal* **101**, 1287–1296 (2011).
- ¹⁸J. Sneyd, J. M. Han, L. Wang, and et al., "On the dynamical structure of calcium oscillations," *Proceedings of the National Academy of Science* **114**, 1456–1461 (2017).
- ¹⁹J. Keizer and L. Levine, "Ryanodine receptor adaptation and Ca^{2+} -induced Ca^{2+} release-dependent Ca^{2+} oscillations," *Biophysical Journal* **71**, 3477–3487 (1997).
- ²⁰O. Cohen and S. A. Safran, "Physics of spontaneous calcium oscillations in cardiac cells and their entrainment," *Physical Review Letters* **122**, 198101 (2019).
- ²¹B. I. Iaparov, A. S. Moskvina, I. Zahradník, and et al., "Stochastic and deterministic approaches to modelling calcium release in cardiac myocytes at different spatial arrangements of ryanodine receptors," *European Biophysics Journal* **48**, 579–584 (2019).
- ²²B. I. Iaparov, I. Zahradník, A. S. Moskvina, and A. Zahradníková, "In silico simulations reveal that ryr distribution affects the dynamics of calcium release in cardiac myocytes," *Journal of General Physiology* **153**, e202012685 (2021).
- ²³M. B. Cannell, C. H. Kong, M. S. Imtiaz, and et al., "Control of sarcoplasmic reticulum Ca^{2+} release by stochastic ryr gating within a 3d model of the cardiac dyad and importance of induction decay for cicer termination," *Biophysical Journal* **104**, 2149–2159 (2013).
- ²⁴M. Walker, G. B. Williams, T. Kohl, and et al., "Superresolution modeling of calcium release in the heart," *Biophysical Journal* **107**, 3018–3029 (2014).
- ²⁵M. A. Walker, T. Kohl, S. E. Lehnart, and et al., "On the adjacency matrix of ryr2 cluster structures," *PLOS Computational Biology* **11**, e1004521 (2015).
- ²⁶T. R. Kolstad, J. van den Brink, N. MacQuaide, and et al., "Ryanodine receptor dispersion disrupts Ca^{2+} release in failing cardiac myocytes," *eLife* **7**, e39427 (2018).
- ²⁷J. W. Shuai and P. Jung, "Optimal intracellular calcium signaling," *Physical Review Letters* **6**, 88 (2002).
- ²⁸I. F. Smith and I. Parker, "Imaging the quantal substructure of single ip_3r channel activity during Ca^{2+} puffs in intact mammalian cells," *Proceedings of the National Academy of Sciences USA* **106**, 6404–6409 (2009).
- ²⁹S. Rüdiger, "Stochastic models of intracellular calcium signals," *Physics Reports* **534**, 39–87 (2014).
- ³⁰S. A. Tiscione, M. Casas, J. D. Horvath, and et al., " Ip_3r -driven increases in mitochondrial Ca^{2+} promote neuronal death in npc disease," *Proceedings of the National Academy of Sciences USA* **118**, e2110629118 (2021).
- ³¹C. Franzini-Armstrong, F. Protasi, and V. Ramesh, "Shape, size, and distribution of Ca^{2+} release units and couplons in skeletal and cardiac muscles," *Biophysical Journal* **77**, 1528–1539 (1999).
- ³²M. E. Hurley, E. White, T. M. D. Sheard, D. Steele, and I. Jayasinghe, "Correlative super-resolution analysis of cardiac calcium sparks and their molecular origins in health and disease," *Open Biology* **13**, 230045 (2023).
- ³³D. Baddeley, I. D. Jayasinghe, L. Lam, and et al., "Optical single-channel resolution imaging of the ryanodine receptor distribution in rat

- cardiac myocytes," *Proceedings of the National Academy of Science* **106**, 22275–22280 (2009).
- ³⁴I. Jayasinghe, A. H. Clowsley, R. Lin, and et al., "True molecular scale visualization of variable clustering properties of ryanodine receptors," *Cell Reports* **22**, 557–567 (2018).
- ³⁵X. Shen, J. den Brink, Y. Hou, and et al., "3d dstorm imaging reveals novel detail of ryanodine receptor localization in rat cardiac myocytes," *The Journal of Physiology* **597**, 399–418 (2019).
- ³⁶G. Hernandez-Hernandez, J. Myers, E. Alvarez-Lacalle, and Y. Shiferaw, "Nonlinear signaling on biological networks: The role of stochasticity and spectral clustering," *Physical Review E* **95**, 032313 (2017).
- ³⁷H.-Y. Jiang and J. He, "Nonlinear signal transduction network with multi-state," *Chinese Physics B* **30**, 118703 (2021).
- ³⁸Z.-X. Gao, T.-T. Li, H.-Y. Jiang, and J. He, "Calcium oscillation on homogeneous and heterogeneous networks of ryanodine receptor," *Physical Review E* **107**, 024402 (2023).
- ³⁹D. Eisner, E. Neher, H. Taschenberger, and G. Smith, "Physiology of intracellular calcium buffering," *Physiological Reviews* **103**, 2767–2845 (2023).
- ⁴⁰D. Terentyev, S. Viatchenko-Karpinski, I. Györke, and et al., "Calsequestrin determines the functional size and stability of cardiac intracellular calcium stores: Mechanism for hereditary arrhythmia," *Proceedings of the National Academy of Science* **100**, 11759–11764 (2003).
- ⁴¹E. Damiani and A. Margreth, "Characterization study of the ryanodine receptor and of calsequestrin isoforms of mammalian skeletal muscles in relation to fibre types," *Journal of Muscle Research & Cell Motility* **15**, 86–101 (1994).
- ⁴²H. Chen, G. Valle, S. Furlan, and et al., "Mechanism of calsequestrin regulation of single cardiac ryanodine receptor in normal and pathological conditions," *Journal of General Physiology* **142**, 127–136 (2013).
- ⁴³Z. Sun, L. Wang, L. Han, and et al., "Functional calsequestrin-1 is expressed in the heart and its deficiency is causally related to malignant hyperthermia-like arrhythmia," *Circulation* **144**, 788–804 (2021).
- ⁴⁴L. Zhang, J. Kelley, G. Schmeisser, Y. M. Kobayashi, and L. R. Jones, "Complex formation between junctin, triadin, calsequestrin, and the ryanodine receptor: proteins of the cardiac junctional sarcoplasmic reticulum membrane," *Journal of Biological Chemistry* **272**, 23389–23397 (1997).
- ⁴⁵I. Györke, N. Hester, L. R. Jones, and S. Györke, "The role of calsequestrin, triadin, and junctin in conferring cardiac ryanodine receptor responsiveness to luminal calcium," *Biophysical Journal* **86**, 2121–2128 (2004).
- ⁴⁶N. A. Beard, M. M. Sakowska, A. F. Dulhunty, and D. R. Laver, "Calsequestrin is an inhibitor of skeletal muscle ryanodine receptor calcium release channels," *Biophysical Journal* **82**, 310–320 (2002).
- ⁴⁷I. Györke, N. Hester, L. R. Jones, and S. Györke, "The role of calsequestrin, triadin, and junctin in conferring cardiac ryanodine receptor responsiveness to luminal calcium," *Biophysical Journal* **86**, 2121–2128 (2004).
- ⁴⁸N. Liu, N. Rizzi, L. Boveri, and S. G. Priori, "Ryanodine receptor and calsequestrin in arrhythmogenesis: what we have learnt from genetic diseases and transgenic mice," *Journal of Molecular and Cellular Cardiology* **2**, 46 (2009).
- ⁴⁹E. T. Sibbles, H. M. M. Waddell, V. Mereacre, P. P. Jones, and M. L. Munro, "The function and regulation of calsequestrin-2: implications in calcium-mediated arrhythmias," *Biophysical Reviews* **14**, 329–352 (2022).
- ⁵⁰J. G. Restrepo, J. N. Weiss, and A. Karma, "Calsequestrin-mediated mechanism for cellular calcium transient alternans," *Biophysical Journal* **95**, 3767–3789 (2008).
- ⁵¹D. X. P. Brochet, D. Yang, A. D. Maio, W. J. Lederer, C. Franzini-Armstrong, and H. Cheng, "Ca²⁺ blinks: Rapid nanoscopic store calcium signaling," *Proceedings of the National Academy of Sciences* **102**, 3099–3104 (2005).
- ⁵²M. A. Colman, E. Alvarez-Lacalle, B. Echebarria, D. Sato, H. Sutanto, and J. Heijman, "Multi-scale computational modeling of spatial calcium handling from nanodomain to whole-heart: Overview and perspectives," *Frontiers in Physiology* **13** (2022), 10.3389/fphys.2022.836622.
- ⁵³T. R. Shannon, F. Wang, J. Puglisi, C. Weber, and D. M. Bers, "A mathematical treatment of integrated ca dynamics within the ventricular myocyte," *Biophysical Journal* **87**, 3351–3371 (2004).
- ⁵⁴M. D. Stern, L.-S. Song, H. Cheng, J. S. Sham, H. T. Yang, K. R. Boheler, and E. Rios, "Local control models of cardiac excitation-contraction coupling: a possible role for allosteric interactions between ryanodine receptors," *J. Gen. Physiol.* **113**, 469–489 (1999).
- ⁵⁵D. Sato and D. M. Bers, "How does stochastic ryanodine receptor-mediated ca leak fail to initiate a ca spark?" *Biophys J* **101**, 2370–9 (2011).
- ⁵⁶D. Sato, T. R. Shannon, and D. M. Bers, "Sarcoplasmic reticulum structure and functional properties that promote long-lasting calcium sparks," *Biophysical Journal* **110**, 382–390 (2016).
- ⁵⁷H. Park, I. Y. Park, E. Kim, and et al., "Comparing skeletal and cardiac calsequestrin structures and their calcium binding: a proposed mechanism for coupled calcium binding and protein polymerization," *J. Biol. Chem.* **279**, 18026–18033 (2004).
- ⁵⁸C. Kettlun, A. González, E. Ríos, and M. Fill, "Unitary ca²⁺ current through mammalian cardiac and amphibian skeletal muscle ryanodine receptor channels under near-physiological ionic conditions," *Biophysical Journal* **85**, 3494–3509 (2003).
- ⁵⁹R. Mejia-Alvarez, C. Kettlun, E. Ríos, M. Stern, and M. Fill, "Unitary ca²⁺ current through cardiac ryanodine receptor channels under quasi-physiological ionic conditions," *Biophysical Journal* **113**, 177–186 (1999).
- ⁶⁰S. Galice, Y. Xie, Y. Yang, D. Sato, and D. M. Bers, "Size matters: Ryanodine receptor cluster size affects arrhythmogenic sarcoplasmic reticulum calcium release," *Journal of the American Heart Association* **7**, e008724 (2018).
- ⁶¹Y. Xie, Y. Yang, S. Galice, D. M. Bers, and D. Sato, "Size matters: Ryanodine receptor cluster size heterogeneity potentiates calcium waves," *Biophysical Journal* **116**, 530–539 (2019).
- ⁶²M. Naraghi and E. Neher, "Linearized buffered ca²⁺ diffusion in microdomains and its implications for calculation of [ca²⁺] at the mouth of a calcium channel," *The Journal of Neuroscience* **17**, 6961–6973 (1997).
- ⁶³H. Y. Jiang and J. He, "Three-dimensional cytoplasmic calcium propagation with boundaries," *Commun. Theor. Phys.* **10**, 105–111 (2021).
- ⁶⁴G. D. Smith, "Analytical steady-state solution to the rapid buffering approximation near an open ca²⁺ channel," *Biophysical Journal* **71**, 3064–3072 (1996).
- ⁶⁵G. D. Smith, J. E. Keizer, M. D. Stern, W. J. Lederer, and H. Cheng, "A simple numerical model of calcium spark formation and detection in cardiac myocytes," *Biophysical Journal* **75**, 15–32 (1998).
- ⁶⁶J. Wagner and J. Keizer, "Effects of rapid buffers on ca²⁺ diffusion and ca²⁺ oscillations," *Biophysical Journal* **67**, 447–456 (1994).
- ⁶⁷D. M. Bers and V. M. Stiffel, "Ratio of ryanodine to dihydropyridine receptors in cardiac and skeletal muscle and implications for e-c coupling," *American Journal of Physiology-Cell Physiology* **264**, C1587–C1593 (1993).
- ⁶⁸R. Hinch, J. L. Greenstein, A. J. Tanskanen, L. Xu, and R. L. Winslow, "A simplified local control model of calcium-induced calcium release in cardiac ventricular myocytes," *Biophysical Journal* **87**, 3723–3736 (2004).
- ⁶⁹M. S. Jafri, "Cardiac ca²⁺ dynamics: the roles of ryanodine receptor adaptation and sarcoplasmic reticulum load," *Biophysical Journal* **74**, 1149 (1998).
- ⁷⁰A. Mahajan, Y. Shiferaw, D. Sato, A. Baher, R. Olcese, L. H. Xie, and et al., "A rabbit ventricular action potential model replicating cardiac dynamics at rapid heart rates," *Biophysical Journal* **94**, 392–410 (2008).
- ⁷¹J. Wei, J. Yao, D. Belke, W. Guo, and S. W. Chen, "Ca²⁺-cam dependent inactivation of ryr2 underlies ca²⁺ alternans in intact heart," *Circulation research* **128**, e63–e83 (2021).
- ⁷²H. Cheng, M. R. Lederer, W. J. Lederer, and M. B. Cannell, "Calcium sparks and ca²⁺ waves in cardiac myocytes," *American Journal of Physiology-Cell Physiology* **270**, C148–C159 (1996).
- ⁷³I. Györke and S. Györke, "Regulation of the cardiac ryanodine receptor channel by luminal ca²⁺ involves luminal ca²⁺ sensing sites," *Biophysical Journal* **75**, 2801–2810 (1998).
- ⁷⁴M. D. Stern, "Theory of excitation-contraction coupling in cardiac muscle," *Biophysical Journal* **63**, 497–517 (1992).